



Modified Vector-Controlled DFIG Wind Energy System Using Robust Model Predictive Rotor Current Control

Abdelkader Achar¹ · Youcef Djeriri¹ · Habib Benbouhenni² · Riyadh Bouddou³ · Z. M. S. Elbarbary^{4,5}

Received: 23 July 2023 / Accepted: 8 July 2024
© The Author(s) 2024

Abstract

As wind energy (WE) technologies become more prevalent, there are significant concerns about the electrical grid's stability. Despite their many advantages, a WE system based on a doubly fed induction generator is vulnerable to power grid disruptions. Due to being built on traditional controllers, the generator systems with standard vector control (VC) cannot resist disturbances. This paper seeks to provide a novel VC that is resistant to outer perturbations. For this purpose, a finite state space model predictive control (FS-MPC) is utilized instead of the internal current loop of the standard VC. The objective of the proposed system is to minimize the error between the measured currents and their reference values and, also, reduces the total harmonic distortion (THD) of the current. The cost function can optimize this requirement, which reduces the computation time. The VC-FS-MPC was implemented using the MATLAB, where a 1.5-MW generator operating under different conditions was used. The necessary graphical and numerical results were extracted to show the efficiency, effectiveness, and ability of the VC-FS-MPC to improve the characteristics of the studied energy system. The results show the flexibility and distinctive performance of the VC-FS-MPC in the various tests used, as the THD of stator current was reduced in the second test compared to the first test by an estimated percentage of 61.79%. Moreover, the THD of rotor current was reduced compared to the first test by an estimated percentage of 23.56%. These ratios confirm the effectiveness of the VC-FS-MPC in improving the characteristics of the proposed system.

Keywords Doubly fed induction generators · Vector control · Wind energy · Finite state space model predictive control

List of Symbols

✉ Habib Benbouhenni
habib.benbouhenni@nisantasi.edu.tr

Abdelkader Achar
abdelkader.achar@univ-sba.dz

Youcef Djeriri
youcef.djeriri@univ-sba.dz

Riyadh Bouddou
riyadh.bouddou@ieee.org

Z. M. S. Elbarbary
albrbry@kku.edu.sa

FS-MPC Finite state space model predictive control
VC Vector control
WE Wind energy
PC Predictive control
WS Wind speed
PWM Pulse width modulation
MPPT Maximum power point tracking
THD Total harmonic distortion
DPC Direct power control
PI Proportional-integral controller
DFIG Doubly fed induction generator
STC Super-twisting control

¹ Intelligent Control and Electrical Power Systems Laboratory, Department of Electrotechnics, Faculty of Electrical Engineering, Djillali Liabes University, Sidi Bel-Abbes, Algeria

² Department of Electrical & Electronics Engineering, Faculty of Engineering and Architecture, Nisantasi University, 34481742 Istanbul, Turkey

³ Department of Electrical Engineering, Institute of Technology, University Center of Naama, Naama, Algeria

⁴ Center for Engineering and Technology Innovations, King Khalid University, Abha 61421, Saudi Arabia

⁵ Department of Electrical Engineering, College of Engineering, King Khalid University, KSA, P.O. Box 394, Abha 61421, Saudi Arabia



SMC	Sliding mode control
NA	Neural algorithm
FL	Fuzzy logic
MLI	Multi-level inverter
SSE	Steady-state error
PSO	Particle swarm optimization
MPC	Model predictive control
RSC	Rotor side converter
GSC	Grid side converter
P_s	Active power
Q_s	Reactive power

1 Introduction

Electrical energy (EE) is now the beating heart of any economy, as it is considered the main engine for development in societies. At present, this energy has penetrated daily human life, and it has become impossible to abandon it, as every day, the demand for it increases, especially in the summer when energy consumption reaches its highest peak in all countries. Using traditional sources such as coal or gas to generate this energy leads to the emission of toxic gases such as carbon dioxide. The emission is harmful to the environment and human health. In addition, in recent years, a terrible rise in temperature and a decrease in the level of precipitation have been observed due to the unwanted phenomenon of global warming. To overcome global warming, protect the environment, and reduce the severity of toxic gases, the solution lies in using renewable energies to generate EE. Using renewable energies as a suitable solution helps significantly increase EE production and protect the environment. Also, the use of renewable energies helps significantly reduce the cost of producing and consuming EE [1, 2]. Renewable energies are free natural energies that are always present and endless. They can be exploited to produce EE easily and at the lowest cost. These renewable energies are diverse, including wind, sun, sea waves, sea currents, and geothermal heat. All of these energies are clean, free, easy to use, and protect the environment from unwanted risks. The principle of generating EE from these sources varies from one type to another. For example, photovoltaic cells are used in the case of solar energy, and electrical generators are used in both wind energy (WE) and sea waves. The use of these sources helps greatly to meet the increasing demand for EE and to reduce the severity of the use of undesirable traditional sources.

Traditionally, WE is one of the most prominent renewable energies that has been relied upon as an alternative solution to overcome the problems and defects of traditional energy systems and meet the increasing demand for EE [3]. This energy is one of the easiest, most effective, and simplest sources used

in generating EE. WE is considered an inexpensive source, available throughout the year, and clean, as its use leads to the absence of the spread of toxic gases and thus preserves the environment. Also, the use of renewable energies in general, especially WE, reduces the costs of transmission and distribution of EE, as it greatly helps in the widespread spread of EE.

To exploit WE to generate EE, turbines are used for this purpose. The role of these turbines is to convert WE into mechanical energy, as we find wind turbines with a horizontal axis and wind turbines with a vertical axis. The difference between these two types lies in the form, cost, energy output, and yield. In most turbines, blades are used, and one, two, or three blades can be used. Wind turbines are used in the form of farms called wind farms to generate EE. Using turbines in groups creates winds between them, as these winds significantly reduce the turbines' yield. Also, wind farms should not be placed in the path of migrating birds. All of these are among the most prominent problems and disadvantages of wind turbines.

In recent years, new turbine technology has emerged that is used to generate EE and overcomes the disadvantages and problems of traditional turbines. This technology is called multi-rotor wind turbines (MRWTs) [4], where several turbines are used to form a single turbine. The use of this technology leads to a significant reduction in the area of wind farms, which leads to reducing the costs of implementing wind farms [5]. However, the use of this technology contributes to increasing the energy gained from the wind and overcoming the wind generated between the turbines in wind farms. This technology has been discussed in detail, with the negatives and positives mentioned, in several scientific works [6, 7].

The use of WE to generate EE is completely different from the use of solar energy in terms of principle, costs, costly components of generating EE, maintenance, ease of implementation, and complexity. In WE, machines called electric generators are used, as their role lies in converting the energy gained from the wind into EE. These generators are diverse, including induction generators [8], synchronous generators [9], direct current generators [10], and doubly fed induction generators (DFIGs) [11]. The DFIGs are considered one of the most prominent and most widespread generators in wind farms on land and at sea because of its advantages compared to other generators, as it is considered one of the best solutions in the case of variable wind speeds (WSs). In this application, DFIGs are frequently used as electric machines because they include a stator connected directly to the grid and a rotor connected to the grid through two static converters [12, 13]. The prototype device used in WE conversion systems (WECSs) was SCIGs (squirrel cage induction generators), which were used in nearly all wind generators [14]. Compared to other machines, this machine has various drawbacks,

including fixed mechanical speed and power compensation. When this machine is connected directly to the power grid, it can be inferred that its efficiency will be minimized and its operating range will be more restricted [13].

A new generator with variable rotor speed capability was created using power electronics. A DFIG has a favorable cost–benefit ratio since it can process around 30% of the rated power and has smaller and less expensive components than a total electronic power converter of the same power output rating [13]. In the field of control, several control strategies have been used to control DFIG, and these strategies differ in principle, simplicity, ease of implementation, cost, number of gains, robustness, and performance. Vector control (VC) [15], direct power control (DPC) [16], sliding mode control (SMC) [17], direct torque control (DTC) [18], field-oriented control (FOC) [19], intelligent control [20], synergetic control (SC) [21], predictive control (PC) [22], super-twisting control (STC) [23], fractional-order control [24], and backstepping control (BC) [25] are all methods for the control of active (P_s) and reactive power (Q_s). All control strategies can be classified into four families, where the first family is represented by linear control strategies such as DPC and DTC, which rely on the use of two hysteresis comparators to control the characteristic quantities [18]. Simplicity, rapid dynamic response, and ease of implementation are among the most prominent features of linear control strategies [16, 18]. The second family is represented by intelligent strategies such as fuzzy logic (FL) and genetic algorithms, where ease of implementation, robustness, and accuracy are among the most prominent features of this family [26]. Also, smart strategies rely heavily on experience and do not require knowledge of the mathematical form of the system under study, which makes them give good results in the event of a malfunction in the system. The third family is represented by nonlinear strategies, which are strategies different from linear strategies in terms of principle, idea, ease, durability, cost, and simplicity. Nonlinear strategies are considered more robust than linear strategies, as they are characterized by complexity and difficulty of implementation compared to linear strategies [22, 23]. Moreover, there are a significant number of gains in these nonlinear strategies such as the BC technique, which makes them difficult to adjust. Also, nonlinear strategies are related to the mathematical model of the carefully studied system, which makes them difficult and expensive to apply in the case of complex systems. Relying on the mathematical model of the system makes nonlinear strategies give unsatisfactory results in the event of a defect in the system under study, which is undesirable. Using nonlinear strategies to control the DFIG, pulse width modulation (PWM) or space vector modulation (SVM) is used to control the generator inverter, where the necessary control pulses are generated from reference voltage values. The former is calculated based on the power error

using nonlinear strategies. However, hybrid strategies represent the fourth family, as this family relies on combining different strategies to control DFIG. This family is characterized by outstanding performance and high durability compared to other families [27]. Among the most prominent of these hybrid strategies can be mentioned the BC-SMC strategy [28], SC-SMC technique [29], fractional-order neural control [30], fractional-order FL control [31], neural DPC technique [32], and SC-STC technique [33]. Despite the distinctive performance of these hybrid strategies, they have many drawbacks, such as complexity, the presence of a significant number of gains, difficulty in achieving, expensive, and their reliance on estimating capabilities, which makes them slightly affected in the event of a malfunction in the machine.

In the field of DFIG control, the traditional VC technique is one of the most widely used strategies for power control, as it relies on the use of a proportional-integral (PI) controller in order to control power [34], where the DC link voltage is controlled by the GSC, and the P_s and Q_s are controlled by the RSC. The direct and indirect VC techniques are the most prominent types of this control [35, 36], as they differ in terms of the degree of complexity, simplicity, robustness, and results obtained. In [37], the indirect method of the VC technique is better than the direct method in reducing the power ripples and the total harmonic distortion (THD) value of the current.

In general, the direct VC technique relies on using two PI controllers to control the DFIG power, and four PI controllers are used for the indirect VC technique [38]. The PI controller parameters significantly influence the performance of this control. The parameters of the PI controller greatly affect the performance of this control, which makes it provide unsatisfactory results in terms of power quality and current of the power system. As is known, using a PI controller gives a fast dynamic response, but it is greatly affected by changes in system parameters, which is undesirable. The use of PI makes the VC strategy less efficient and less effective in the event of a malfunction in the system under study. Differential evolution, particle swarm optimization (PSO), barrier function adaptive SMC technique, and bacterial foraging are some of the PI controller tuning methods proposed in the literature [39–42]. These techniques are designed according to the linearized DFIG model around an operational node. The typical vector-controlled DFIG system performance is impaired by significant perturbations, such as three-phase faults, as the DFIG system is a nonlinear system to a high degree. To combat the nonlinear behavior of the DFIG system, nonlinear controllers were proposed [43–49]. In [50], the third-order SMC (TOSMC) technique was used to improve the characteristics of the direct VC strategy of the 1500 kW DFIG-based MRWT system, where two TOSMC controllers were used. In this proposed strategy, TOSMC controllers were used

instead of using traditional controllers, as the outputs of these proposed controllers are reference voltage values. These reference values are used by the PWM strategy to generate the pulses needed to operate the RSC of DFIG. The advantage of direct VC-TOSMC control is simplicity, robustness, ease of operation, and fast dynamic response. Also, the proposed strategy features a small number of gains which makes it easy to adjust and the dynamic response can be easily changed. However, this proposed strategy has a negative side, which is the reliance on the mathematical model of the machine and the use of power estimation, which makes it slightly affected if the machine parameters change. The proposed strategy was implemented in the MATLAB environment, where the results obtained were compared with the traditional strategy and some existing works in terms of response time, power ripple reduction ratio, and THD value of current. A variable WS was used to complete the proposed study while proposing different tests to operate the generator. Moreover, the direct VC-TOSMC strategy gave excellent results in terms of current quality, THD value of current, and response time of energies compared to the direct VC technique. Another strategy is a modified SMC (MSMC) technique used in [51] to overcome direct VC technique problems. In this new strategy, all conventional controllers are eliminated and replaced with the MSMC technique. This new controller results in increased robustness, reduced power ripples, and improved current quality. Also, improved dynamic response compared to the direct VC technique. Moreover, the direct VC-MSMC strategy is inexpensive and simple. It can be easily implemented with the possibility of adjusting the result easily due to the presence of a small number of parameters. Also, the PWM technique was used as a suitable solution in this work to simplify the system and reduce its total cost. The PWM technique inputs are the reference values for the voltages generated by the MSMC controllers, and the outputs are the pulses needed to operate the RSC of DFIG. The MATLAB environment was used to verify the validity, robustness, performance, and efficiency of the proposed strategy, where the numerical and graphical results were compared with the traditional strategy. Simulation results show the superiority of the proposed strategy over the traditional strategy in terms of significantly improving system characteristics and increasing robustness. Also, it is noted that the THD value of the stream is very low in the case of the proposed strategy compared to the traditional strategy, which indicates that the quality of the stream is better in the case of the proposed control. However, this proposed strategy has a negative side, represented in its use of the process of estimating capabilities and its reliance on the mathematical model of the system, which is undesirable, making the proposed strategy affected if the system parameters change and this is what the robustness test shows. In [52], the synergetic-SMC (SSMC) technique is implemented in the direct VC technique in order to control

the DFIG energy. In this work, an SSMC technique was used in place of the PI controller, where this nonlinear controller is used to calculate the voltage reference values and generate the pulses necessary to control the inverter using the PWM strategy. The proposed strategy has been applied to the RSC of the DFIG-based MRWT system. The proposed strategy is characterized by robustness, simplicity, ease of implementation, inexpensive, and outstanding performance compared to the traditional strategy. Also, there are a few gains that makes it easy to adjust the dynamic power response. The MATLAB environment was used to implement the proposed strategy, using several tests to study the behavior of the proposed strategy compared to traditional control. This new strategy has the great ability to improve the characteristics of the generation system compared to the classical control, and this is proven by the simulation results performed. Despite the outstanding performance of the proposed strategy, it is noted that there are ripples at the power and current levels, especially in the durability test, which proves that the proposed strategy was affected by the change in the DFIG parameters. This effect can be attributed to the use of machine power estimation. Therefore, it is necessary to search for a strategy that is characterized by high durability and is not affected by changes in system parameters, as other conditions must be met such as simplicity, ease of implementation, small number of gains, inexpensive, and distinguished performance in reducing energy ripples and increasing the quality of the current. In [53], STCs are used as a better solution to improve the indirect VC control efficiency of DFIG. In addition to using STCs, a three-level adaptive-network-based FL inference system-PWM technique was used to generate the necessary pulses to control the generator inverter. This strategy is characterized by high durability compared to the traditional control. A variable WS was used to study the behavior of the proposed strategy compared to the traditional strategy. Also, the machine parameters were changed and the behavior change of the proposed strategy compared to the traditional strategy was studied. The graphical and numerical simulation results obtained from the MATLAB environment show that the proposed strategy has a distinctive performance compared to the traditional strategy in terms of reducing energy ripples, reducing the value of THD of current, and being affected by DFIG parameter changes. In the durability test, it is noted that the power ripples and the THD of the current value have increased in the case of the two controls, which is undesirable. High energy fluctuations negatively affect the network and make the operation of the energy system unstable, as it may lead to unwanted malfunctions in the system. In addition to the high energy ripples, the life span of the automated system is significantly reduced. In [54], a four-level PWM-FL technique and a neural algorithm (NA) are used to improve the characteristics of the direct VC technique for DFIG control. It is applied to a power generation

system that uses a double-rotor wind turbine system, where a four-level inverter is used to generate the necessary pulses using the smart strategy. In addition, a PI controller based on an NA technique is used to control the P_s and Q_s of the DFIG. The proposed strategy is characterized by complexity compared to the traditional strategy. But it has great robustness compared to the traditional strategy. This strategy was implemented using simulation with a generator with a capacity of 1.5 megawatts, where the simulation results showed the high performance of the proposed strategy compared to the conventional control in terms of steady-state error (SSE), overshoot, time response, etc. Another solution has shown its high efficiency in improving direct VC strategies using a multi-level inverter (MLI) [55–58]. Using an MLI greatly improves the current quality and reduces the THD value. Also, the use of an MLI reduces power ripples significantly. The disadvantage of using an MLI is the complexity, difficulty of control, high cost, and difficult maintenance, which creates undesirable problems. Also, smart strategies based on NA techniques and FL techniques were used to generate the necessary control pulses in the inverter to improve the VC strategies [59, 60], as the use of these smart strategies confirms the significant increase in the robustness of the generation system. This is shown in the presented results, especially in the THD value of current and the power ripple ratio compared to the conventional control. The disadvantage of using these smart strategies is that there are no mathematical rules that control their use but rather depend on the user's experience only. The indirect strategy of the VC technique is discussed in [61] using the combination of the PSO algorithm, PI controller, and STC technique, where the PWM technique is used to control the DFIG inverter. The PI-STC-PSO controller was used instead of the PI controller, where four controllers were used for this purpose. This new control is characterized by complexity and difficulty in achieving compared to some other controls, such as the direct and indirect strategy of the VC technique. Also, another negative is the use of power estimation, which makes it affected in the event of a malfunction in the system, which is an undesirable matter that contributes to a significant increase in power ripples and current. However, it provided very acceptable results of great importance in the field of renewable energies, especially in the value of THD of current, where the reduction percentage reached 96% compared to conventional control. In [60], the author has calculated the indirect strategy parameters of a VC technique based on an STC controller using the PSO algorithm to control the energies of a generation system based on using the DFIG. The indirect VC-STC-PSO strategy modifies the traditional indirect VC technique, where the PI controller is removed and replaced with an STC-PSO controller. Also, the PWM technique was used to control the DFIG inverter. The resulting control is complex, expensive, and difficult to achieve compared to conventional control.

The proposed strategy uses capacity estimation, which makes it affected in the event of a malfunction in the energy system. This proposed strategy was implemented using the MATLAB environment, and the results obtained were compared with the traditional strategy in terms of robustness and reference tracking. The results obtained prove that the proposed strategy is characterized by high performance, great durability, and great efficiency in reducing energy ripples and reducing the value of THD of current compared to the traditional technique.

The paper's main focus in [39] is implementing a damping controller for the DFIG system. The investigation also focuses on how the tunable damping controller affects the converter ratings of the DFIG system. As the fundamental concept in the paper [40], it involves using sensitivity analysis to find the essential factors first, the unified dominant control parameters (UDCPs), to reduce the difficulty of the optimization. The PSO technique is then used to determine the optimal values based on these selected parameters to achieve the control objective. The simulation analysis and comparative studies prove the accuracy of the system. Using a sophisticated differential evolution method to adjust the parameters, [41] aims to maximize the performances of vector-controlled DFIGs in a multi-machine electrical system under problematic situations. The goal of [22] is to build a novel VC technique that is resistant to outside perturbations. A multi-machine electrical system reference model is used to test the proposed barrier function adaptive SMC technique under various operating scenarios. Simulation results from previous studies show that the optimized system has improved stability and overall performance and can traverse faults.

As a result of the stochastic WS nature [63, 64], variable power production has a significant impact on WES. Robust control is thus the most efficient method for managing DFIG systems. Predictive control (PC) technique has been used to regulate the DFIG system since it is a reliable control approach [65, 66]. Compared to traditional strategies, the PC technique is considered among the strategies that have a distinctive and effective performance in improving the characteristics of systems. Also, it is characterized by great durability against changes in the parameters of the system under study, as it gives very satisfactory results in terms of ripples and the value of THD of current. Nevertheless, the model PC (MPC) technique minimizes the control rule to ensure that the output achieves the references by using its model to forecast future behavior. Generalized PC technique that uses a transfer function as a system model to derive the law of control [67] and continuous-time PC technique [12] are some examples of the many PC techniques for DFIGs, such as MPC technique, that use nonlinear models [65, 68], and finite the rotor or stator [45, 69]. Given its low processing cost compared to the nonlinear ones and its capability to directly

process the coupling and the flux components, the state space model is the most practical among these PC techniques [66]. For a synchronous reluctance motor system, [43] a model-based predictive current control is suggested with the same control in the referenced work [44]. It detailed how a DFIG functions with THD of voltage in a reference frame with synchronization. The finite control strategy-based model PC technique for the wind generator is presented in [45] and is time efficient. The commutation states of the RSC are used as direct control in this approach. In this way, the converter can obtain the improved control action directly. Based on the fictitious algebraic Riccati equation, the paper cited in [46] proposes an analytical technique to design the weighting matrix under the same control concept. The proposed technique ensures system control stability. The paper [47] presents a robust control of low complexity based on MPC techniques of the rotor current of a DFIG operating with a direct matrix converter. This is attractive because the lack of a heavy and delicate DC linkage capacitor improves reliability. Speed control is performed using feedforward control. For a grid-connected doubly fed induction motor, reference [48] proposes a speed sensorless control strategy known as finite control set current PC technique, which uses a modified fictive resistive quantity based on a model reference adaptive system (MRAS). The proposed MPC technique in [49] considers the converter-based system model to forecast the prospective performance of the controlled parameters. The system model serves as the basis for the predictive dead-time control, which determines the ideal voltage vector to guarantee zero SSE. Finally, as a result of these previous studies, the proposed control in our paper is built based on the finite control strategy-based MPC technique.

The finite control strategy-based MPC technique is introduced in [43–49]. To obtain effective control of various disturbances and increased robustness, the conventional VC technique-controlled DFIG system is changed, and finite control strategy-based MPC technique is used to build the present control loop. To obtain a quicker convergence than the outer control loop, the finite control strategy-based MPC technique is added to the inner current loop.

The following are the paper's main contributions:

- A suggested modified vector using a robust model predictive rotor current control (MV-FCS-MPC) technique for a wind turbine is suggested in this article. The proposed composite predictive model control combines finite control strategy-based MPC technique for inner current loop dynamics with PI control for the outer loop. The internal current loop control of the GSC and the RSC is created using finite control strategy-based MPC technique.
- The MV-FCS-MPC technique can perform optimum control, explicitly handle restrictions, and directly provide commutation signals for the rotor and grid side converter.

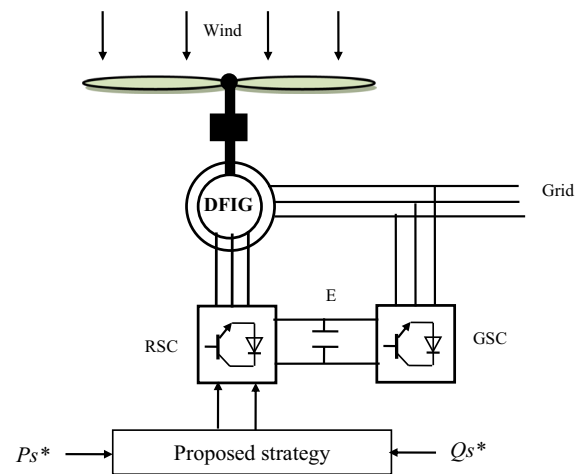


Fig. 1 Proposed system

- The controller can withstand a variety of disturbances, including parametric changes and shifting WSs.
- Because of the shorter calculation times, the finite control strategy-based MPC technique may use larger prediction horizons, which improves control performance.

This paper is structured in the following sections: Sect. 2 describes the mathematical model of the WE system. In Sect. 3, the proposed strategy is given to control the RSC and GSC of DFIG, where the necessary equations are given and figures are used to illustrate the principle of the proposed strategy. The simulations in Sect. 4 show the controller's performance on the wind power system and the power quality improvement under a series of tests. Finally, in Sect. 5, a conclusion is presented.

2 WE System Model

The system studied in this paper is represented in Fig. 1, which consists of a conventional three-blade turbine, a DFIG, and two inverters. In addition to these devices, there is control, which is no less important in its relationship to the quality of the energy produced. In addition, simplicity is one of the most prominent features of this system, which makes it reduce the production bill and energy consumption, which is desirable.

To study any system, it was necessary to first model the system using mathematical equations. Using these equations, the mechanical and electrical parts of the electrical system or machine under study are expressed. Also, these equations are used in simulations to implement the system, where the simulation gives a picture of the system's behavior almost as it is in reality. Therefore, the turbine and generator will be

given the mathematical form because they are the two main elements in the studied system.

In this system proposed for the study, a generator with a capacity of 1.5 MW was used to generate power. This system aims to generate energy from wind and overcome the problems found in traditional systems. In this proposed system, highly efficient control is used with a great ability to reduce energy ripples in the event of a malfunction in the system, such as a change in machine parameters.

The turbine is the cornerstone of the generation system. It comes at the beginning of the generation chain, as it is responsible for converting WE into mechanical energy, a process succinctly described by Eq. (1) [61].

$$P_t = 0.5 \rho \pi R^2 C_p(\lambda, \beta) V^3 \tag{1}$$

The power generated by the turbine is related to a coefficient called the coefficient of power, where this coefficient is related to the pitch of angle (β), and the largest value of this coefficient is 0.59 in the case of an angle of 0. This coefficient is expressed by Eq. (2).

$$C_p(\lambda, \beta) = \frac{46}{100} \left(\frac{151}{\lambda_i} - \frac{58}{100} \beta - \frac{2}{1000} \beta^{2.14} - 13.2 \right) e^{-\frac{18.4}{\lambda_i}} \tag{2}$$

Through Eq. (2), the power factor is affected by another element called the tip speed of ratio (λ). λ has a greater value if β is close to zero. Accordingly, for the calculation λ , Eq. (3) is used for this purpose [62].

$$\lambda_i = \frac{1}{\lambda + 0.02\beta} - \frac{0.003}{\beta^3 + 1} \tag{3}$$

With:

$$\lambda = \frac{R \Omega_t}{V} \tag{4}$$

Using Eq. (1), the torque produced by the turbine can be written as:

$$T_{aer} = \frac{1}{2 \Omega_t} \rho \pi R^2 C_p(\lambda, \beta) V^3 \tag{5}$$

Equation (6) represents the mathematical model for the mechanical transmission of a turbine.

$$\begin{cases} T_m = \frac{T_{aer}}{G} \\ \Omega_m = G \Omega_t \end{cases} \tag{6}$$

The mechanical part of the turbine is represented in Eq. (7), which relates speed and torque.

$$J_{tot} \frac{d\Omega_m}{dt} = T_m - T_{em} - f \Omega_m \tag{7}$$

where f is the friction coefficient, J_{tot} is the moment inertia, and T_{em} is the torque delivered by DFIG.

In a DFIG, the rotor is linked across a transformer and two converters back-to-back, while the stator is directly connected to the three-phase grid. While the GSC regulates the voltage and power factor of the DC link, the RSC supervises the P_s and Q_s [70].

By projecting onto the d-q plane, the DFIG equations associated with the rotating field are given as follows:

The stator and rotor voltages:

$$\begin{cases} V_{sd} = R_s I_{sd} + \frac{d}{dt} \phi_{sd} - \omega_s \phi_{sq} \\ V_{sq} = R_s I_{sq} + \frac{d}{dt} \phi_{sq} + \omega_s \phi_{sd} \\ V_{rd} = R_r I_{rd} + \frac{d}{dt} \phi_{rd} - (\omega_s - \omega_r) \phi_{rq} \\ V_{rq} = R_r I_{rq} + \frac{d}{dt} \phi_{rq} + (\omega_s - \omega_r) \phi_{rd} \end{cases} \tag{8}$$

Stator and rotor magnetic fluxes:

$$\begin{cases} \phi_{sd} = L_s I_{sd} + L_m I_{rd} \\ \phi_{sq} = L_s I_{sq} + L_m I_{rq} \\ \phi_{rd} = L_r I_{rd} + L_m I_{sd} \\ \phi_{rq} = L_r I_{rq} + L_m I_{sq} \end{cases} \tag{9}$$

The P_s and Q_s outputs are given by:

$$\begin{cases} P_s = \frac{3}{2} (V_{sd} I_{sd} + V_{sq} I_{sq}) \\ Q_s = \frac{3}{2} (V_{sq} I_{sd} - V_{sd} I_{sq}) \end{cases} \tag{10}$$

The torque:

$$T_{em} = \frac{3}{2} p \frac{L_m}{L_s} (\phi_{sq} I_{rd} - \phi_{sd} I_{rq}) \tag{11}$$

where s/r are stator/rotor index; V/I are voltage/current; ϕ is flux; R is resistance; L_m is mutual inductance; L_r/L_s are inductance; ω_r/ω_s are rotor/stator pulsation; p is number of the pairs of poles.

We can conclude by assuming negligible stator resistance R_s and a constant stator flux (this condition is guaranteed if the stator of the DFIG is connected to the electrical grid) and orienting the d axis along the stator flux [71, 72]:

$$\begin{cases} \phi_{sq} = 0 \\ \phi_{sd} = \phi_s \end{cases} \tag{12}$$

$$\begin{cases} V_{sd} = 0 \\ V_{sq} = V_s = \omega_s \phi_s \end{cases} \tag{13}$$

$$\begin{cases} \phi_s = L_s I_{sd} + L_m I_{rd} \\ 0 = L_s I_{sq} + L_m I_{rq} \end{cases} \quad (14)$$

From Eq. (14), a relation can be established between the stator and rotor currents as follows:

$$\begin{cases} I_{sd} = \frac{\phi_s}{L_s} - \frac{L_m}{L_s} I_{rd} \\ I_{sq} = -\frac{L_m}{L_s} I_{rq} \end{cases} \quad (15)$$

By replacing in Eq. (9) the stator currents of Eq. (15), we obtain:

$$\begin{cases} \phi_{rd} = \sigma L_r I_{rd} + \frac{L_m}{L_s} \phi_s \\ \phi_{rq} = \sigma L_r I_{rq} \end{cases} \quad (16)$$

with: $\sigma = 1 - \left(\frac{L_m^2}{L_s L_r}\right)$ is the blondel dispersion coefficient.

The rotor current may be rewritten as follows by substituting Eqs. (16) and (15) in Eq. (8):

$$\begin{cases} \frac{dI_{rd}}{dt} = \frac{1}{L_r \sigma} (V_{rd} - R_r I_{rd} + g \omega_s L_r \sigma I_{rq}) \\ \frac{dI_{rq}}{dt} = \frac{1}{L_r \sigma} (V_{rq} - R_r I_{rq} - g \omega_s L_r \sigma I_{rd} - g \frac{L_m V_s}{L_s}) \end{cases} \quad (17)$$

By replacing the stator currents with their values from Eq. (15) in Eq. (10) by adapting Eqs. (13), we obtain the equations for the P_s and Q_s as follows:

$$\begin{cases} P_s = -\frac{3}{2} V_s \frac{L_m}{L_s} I_{rq} \\ Q_s = \frac{3}{2} \left(V_s \frac{\phi_s}{L_s} - V_s \frac{L_m}{L_s} I_{rd} \right) \end{cases} \quad (18)$$

By taking $\phi_s = \frac{V_s}{\omega_s}$ from Eq. (18), the Q_s expression becomes:

$$Q_s = -\frac{3}{2} V_s \frac{L_m}{L_s} I_{rd} + \left(\frac{3 V_s^2}{2 L_s \omega_s} \right) \quad (19)$$

By replacing Eq. (12) in Eq. (11), the couple of the DFIG will have for expression:

$$T_{em} = -\frac{3}{2} p \frac{L_m V_s}{L_s \omega_s} I_{rq} \quad (20)$$

GSC may manage the grid-side displacement factor by limiting the rotor's reactive input power [47]. The control decouples P_s and Q_s by aligning the Park reference frame with the power grid voltage vector as follows:

$$\begin{cases} v_{dg} = v_g \\ v_{qg} = 0 \end{cases} \quad (21)$$

The equations can represent the input filter model in continuous time as follows [71–73]:

$$\begin{cases} \frac{dI_{dg}(t)}{dt} = \frac{1}{L_g} (V_{dg}(t) - R_g \cdot I_{dg}(t) + \omega_s \cdot I_{qg}(t) - V_g) \\ \frac{dI_{qg}(t)}{dt} = \frac{1}{L_g} (V_{qg}(t) - R_g \cdot I_{qg}(t) - \omega_s \cdot I_{dg}(t)) \end{cases} \quad (22)$$

where R_f and L_f are the resistance and inductance of the line filter, respectively. The following state space model can express the input side of the filter:

$$x(t) = A_g x(t) + B_g u(t) + C \quad (23)$$

With:

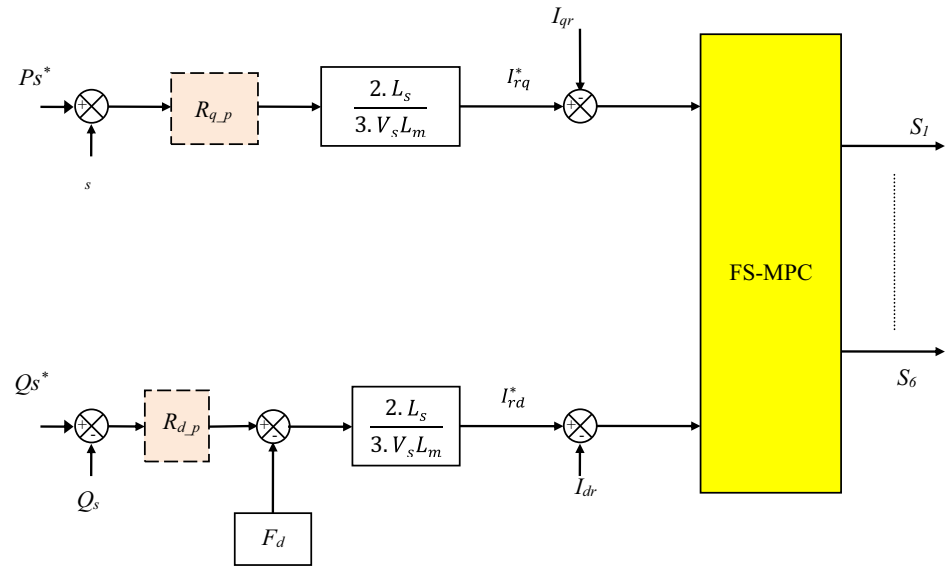
$$\begin{aligned} x(t) &= \begin{bmatrix} I_{dg}(t) \\ I_{qg}(t) \end{bmatrix}, u(t) = \begin{bmatrix} V_{dg}(t) \\ V_{qg}(t) \end{bmatrix}, A_g \\ &= \begin{bmatrix} -R_g/L_g & \omega_s/L_g \\ -\omega_s/L_g & -R_g/L_g \end{bmatrix}, B_g \\ &= \begin{bmatrix} 1/L_g & 0 \\ 0 & 1/L_g \end{bmatrix}, \text{ and } C = \begin{bmatrix} -V_g \\ 0 \end{bmatrix} \end{aligned}$$

3 WE System Control

In this section, a new nonlinear control technique is proposed to control the energy system, and this proposed strategy is used to obtain satisfactory results compared to the traditional strategy and some other works. The proposed strategy relies on the use of both the VC and FS-MPC techniques to create a control characterized by high durability and the ability to reduce energy ripples. This proposed strategy depends on developing and modifying works [74–77], as these works differ in terms of principle, simplicity, complexity, performance, durability, and the results obtained. In this proposed strategy, the PWM strategy or SVM technique is not used to control the inverter. This proposed strategy has been applied to both RSC and GSC of DFIG-based wind turbine systems.

In articles [78–80] and [45, 48, 81, 82], the FS-MPC technique is utilized as a comprehensive system control, overseeing both P_s and Q_s control. Acknowledging that relying on currents for control enhances robustness, improves performance, and reduces energy ripples, our research takes a different approach. The control proposed in our research paper is centered on using the FS-MPC technique as a regulator specifically for rotor currents, not as a complete power controller, and using the PI controller as an external power control loop. This approach resulted in a notable improvement in output power and demonstrated success in all conducted tests. So the proposed strategy is two strategies in a row, where the VC strategy is used to obtain the reference

Fig. 2 Modified RSC control



values of the rotating current based on the reference values of the powers. The stream reference values are inputs to the FS-MPC strategy. The FS-MPC strategy is used to generate the pulses needed to operate the RSC of the DFIG-based wind turbine system. For the GSC of DFIG, the FS-MPC strategy is used to generate the necessary pulses necessary to operate the GSC, where the PI controller is used to control the DC link voltage. PWM or SVM is not used to control the GSC of DFIG, which makes the proposed power system more robust and provides high-quality current.

As it is known, the DFIG-WE system is a stochastic nonlinear system that is sensitive to power line failures, WS fluctuations, and parameter disturbances. The conventional VC technique-controlled DFIG is not resilient. The FS-MPC technique improves the resilience of the VC technique. The control objectives are:

$$\begin{cases} \lim_{x \rightarrow t_F} (i_{dr} - i_{dr_ref}) \rightarrow 0 \\ \lim_{x \rightarrow t_F} (i_{qr} - i_{qr_ref}) \rightarrow 0 \\ \lim_{x \rightarrow t_F} (i_{dg} - i_{dg_ref}) \rightarrow 0 \\ \lim_{x \rightarrow t_F} (i_{qg} - i_{qg_ref}) \rightarrow 0 \end{cases} \quad (24)$$

where t_F is the time required for the simulation. i_{dr_ref} , i_{qr_ref} , i_{dg_ref} , and i_{qg_ref} are the d-q frame's reference currents.

Figure 2 shows a proposed control for a DFIG used in this work for controlling the P_s and Q_s .

where R_{q-p} and R_{d-p} are the P_s and Q_s regulators. F_d is the decoupling compensation.

The FS-MPC strategy used to control the GSC of DFIG is different from the FS-MPC strategy used to control the RSC of DFIG, as the difference lies in the equations and the principle used remains the same. Figure 3 illustrates the

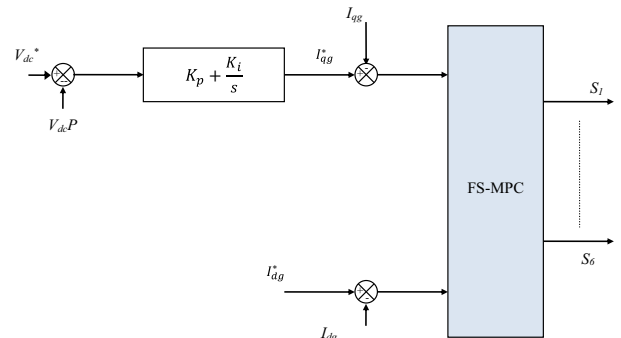


Fig. 3 Modified GSC control

current control diagram of the GSC in the reference frame of Park.

The proposed PC technique uses the ability of a converter to create only a limited number of commutation states. The following formula can be used to describe the voltage equation of the rotor in the synchronous rotation condition [44]:

$$\begin{cases} v_{rd} = R_r i_{rd} + \sigma L_r \frac{d}{dt} i_{rd} - g_i \omega_s \sigma L_r i_{rq} \\ v_{rq} = R_r i_{rq} + \sigma L_r \frac{d}{dt} i_{rq} + g_i \omega_s \sigma L_r i_{rd} + g_i \frac{L_m V_s}{L_s} \end{cases} \quad (25)$$

The GSC currents are analyzed with the grid voltages Park reference frame. In this context, the filter (R_g, L_g) electrical equations may be simplified as follows:

$$\begin{cases} V_{dg} = R_g i_{dg} + L_g \frac{di_{dg}}{dt} - \omega_s L_g i_{qg} + V_g \\ V_{qg} = R_g i_{qg} + L_g \frac{di_{qg}}{dt} - \omega_s L_g i_{dg} \end{cases} \quad (26)$$

In FS-MPC technique, the discrete form of Eqs. (25) and (26), taking the basic “Euler” approach, can be represented as follows:

Table 1 FS-MPC switching states and corresponding output voltage ($\vec{V}_{dq_r-g_j}$)

S_a	S_b	S_c	$V_{\alpha r_j}$ Or $V_{\alpha g_j}$	$V_{\beta r_j}$ Or $V_{\beta g_j}$	\vec{V}_j	$\vec{V}_{dq_r-g_j}$	\vec{V}_{dq_g-j}
0	0	0	0	0	V_0	$V_{dq_r_0}$	$V_{dq_g_0}$
1	0	0	$2V_{dc}/3$	0	V_1	$V_{dq_r_1}$	$V_{dq_g_1}$
1	1	0	$V_{dc}/3$	$V_{dc}/\sqrt{3}$	V_3	$V_{dq_r_2}$	$V_{dq_g_2}$
0	1	0	$-V_{dc}/3$	$V_{dc}/\sqrt{3}$	V_3	$V_{dq_r_3}$	$V_{dq_g_3}$
0	1	1	$-2V_{dc}/3$	0	V_4	$V_{dq_r_4}$	$V_{dq_g_4}$
0	0	1	$-V_{dc}/3$	$-V_{dc}/\sqrt{3}$	V_5	$V_{dq_r_5}$	$V_{dq_g_5}$
1	0	1	$V_{dc}/3$	$-V_{dc}/\sqrt{3}$	V_6	$V_{dq_r_6}$	$V_{dq_g_6}$
1	1	1	0	0	V_7	$V_{dq_r_7}$	$V_{dq_g_7}$

$$\begin{cases} i_{dr}(k+1) = \left(\frac{T_s}{\sigma L_r} (V_{dr}(k) - R_r i_{dr}(k) + g\omega_s \sigma L_r i_{qr}(k)) + i_{dr}(k) \right) \\ i_{qr}(k+1) = \left(\frac{T_s}{\sigma L_r} (V_{qr}(k) - R_r i_{qr}(k) - g\omega_s \sigma L_r i_{dr}(k) - g \frac{L_m V_s}{L_s}) + i_{qr}(k) \right) \end{cases} \quad (27)$$

$$\begin{cases} i_{dg}(k+1) = \left(\frac{T_s}{L_g} (V_{dg}(k) - R_g i_{dg}(k) + \omega_s L_g i_{qg}(k) - V_g) + i_{dg}(k) \right) \\ i_{qg}(k+1) = \left(\frac{T_s}{L_g} (V_{qg}(k) - R_g i_{qg}(k) + \omega_s L_g i_{dg}(k)) + i_{qg}(k) \right) \end{cases} \quad (28)$$

where T_s is the sample period, $i_{dr}(k)$, $i_{dr}(k)$, $i_{qr}(k)$, $i_{dg}(k)$, and $i_{qg}(k)$ are the rotor and filter measured currents, respectively, at kT_s . $V_{dr}(k)$, $V_{qr}(k)$, $V_{dg}(k)$, and $V_{qg}(k)$ are the rotor and filter voltages derived from the optimum voltage vector implemented in the (k) sampling period. They can be found by applying a rotational process of an angle equal to θ_{dq} and $\alpha\beta$ of the voltage vector components as given in Eq. (29) and Table 1.

$$\begin{bmatrix} V_{dr_j}(k) \\ V_{qr_j}(k) \\ V_{dg_j}(k) \\ V_{qg_j}(k) \end{bmatrix} = \begin{bmatrix} \cos(\theta_{dq}(k)) & \sin(\theta_{dq}(k)) \\ -\sin(\theta_{dq}(k)) & \cos(\theta_{dq}(k)) \\ \cos(\theta_{dq}(k)) & \sin(\theta_{dq}(k)) \\ -\sin(\theta_{dq}(k)) & \cos(\theta_{dq}(k)) \end{bmatrix} \begin{bmatrix} V_{\alpha r_j}(k) \\ V_{\beta r_j}(k) \\ V_{\alpha g_j}(k) \\ V_{\beta g_j}(k) \end{bmatrix} \quad (29)$$

Equations (27) and (28) can be written for the multiple possible stator voltage components d and q , $V_{dr_j}(k)$, $V_{qr_j}(k)$, $V_{dg_j}(k)$, and $V_{qg_j}(k)$ of voltage vectors $\vec{V}_{dq_r-g_j}$ by taking the eight commutating state combination of DFIG and

GSC with two combinations leading to a no voltage vector:

$$\begin{cases} i_{dr_j}(k+1) = \left(\frac{T_s}{\sigma L_r} (V_{dr_j}(k) - R_r i_{dr}(k) + g\omega_s \sigma L_r i_{qr}(k)) + i_{dr}(k) \right) \\ i_{qr_j}(k+1) = \left(\frac{T_s}{\sigma L_r} (V_{qr_j}(k) - R_r i_{qr}(k) - g\omega_s \sigma L_r i_{dr}(k) - g \frac{L_m V_s}{L_s}) + i_{qr}(k) \right) \end{cases} \quad (30)$$

$$\begin{cases} i_{dg_j}(k+1) = \left(\frac{T_s}{L_g} (V_{dg_j}(k) - R_g i_{dg}(k) + \omega_s L_g i_{qg}(k) - V_g) + i_{dg}(k) \right) \\ i_{qg_j}(k+1) = \left(\frac{T_s}{L_g} (V_{qg_j}(k) - R_g i_{qg}(k) + \omega_s L_g i_{dg}(k)) + i_{qg}(k) \right) \end{cases} \quad (31)$$

With: $j = 0 \dots 0.7$.

where i_{dr_j} , i_{qr_j} , i_{dg_j} , and i_{qg_j} are the predicted d and q stator and filter current components at the sampling period (k + 1)th when the voltage vector components $V_{\alpha r_j}$, $V_{\beta r_j}$, $V_{\alpha g_j}$, and $V_{\beta g_j}$ are applied during the kth sample period (Table 1).

It is, necessary to predict the dq stator and GSC vector components $\Delta i_{dr_j}(k+1)$, $\Delta i_{qr_j}(k+1)$, $\Delta i_{dg_j}(k+1)$, and $\Delta i_{qg_j}(k+1)$. These errors in current measurements were given as the difference between the reference stator and GSC current vector at the (k)th sampling period and the sampling period future (k + 1)th when the voltage of the stator and the GSC vector $\vec{V}_{dq_r-g_j}(k)$ is applied.

$\Delta i_{dr_j}(k+1)$, $\Delta i_{qr_j}(k+1)$, $\Delta i_{dg_j}(k+1)$, and $\Delta i_{qg_j}(k+1)$ are detailed in Eqs. (24) and (25).

$$\begin{cases} \Delta i_{dr_j}(k+1) = i_{dr}^*(k) - i_{dr_j}(k+1) \\ \Delta i_{qr_j}(k+1) = i_{qr}^*(k) - i_{qr_j}(k+1) \end{cases} \quad (32)$$

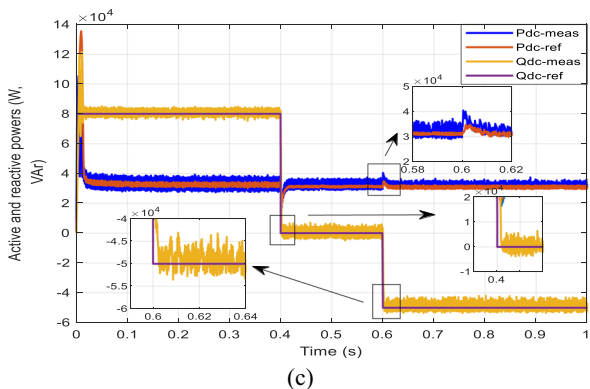
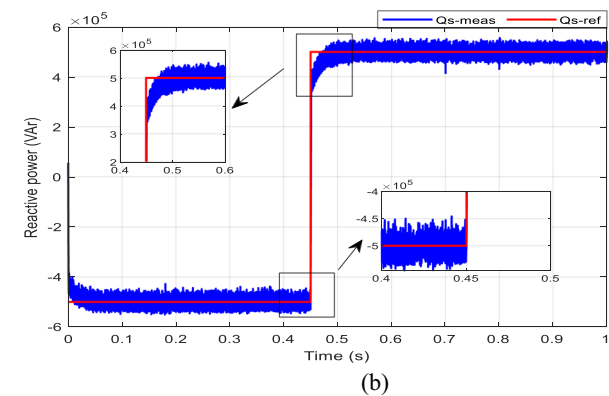
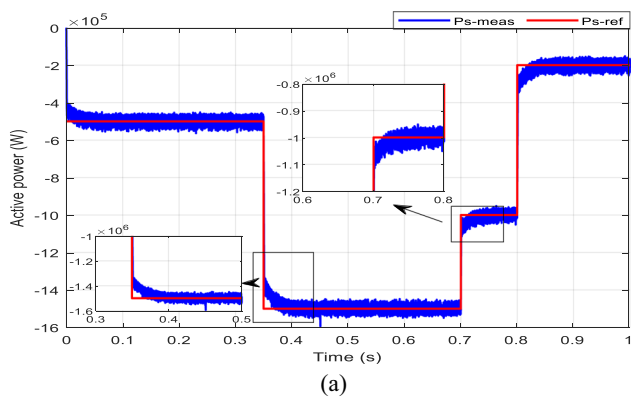


Fig. 4 Step change response in power references: a and b for DFIG and c for DC bus

$$\begin{cases} \Delta i_{dg_j}(k+1) = i_{dg}^*(k) - i_{dg_j}(k+1) \\ \Delta i_{qg_j}(k+1) = i_{qg}^*(k) - i_{qg_j}(k+1) \end{cases} \quad (33)$$

The quality function ensures the good efficiency of the dynamic control. The cost function is calculated for each feasible switching state of the converter for each sampling period, choosing the one with the least error for the following sample period.

Based on Eqs. (32) and (33), a function of cost F is used for the generated stator current and SCG error components to pick the optimum voltage vector, which reduces the errors

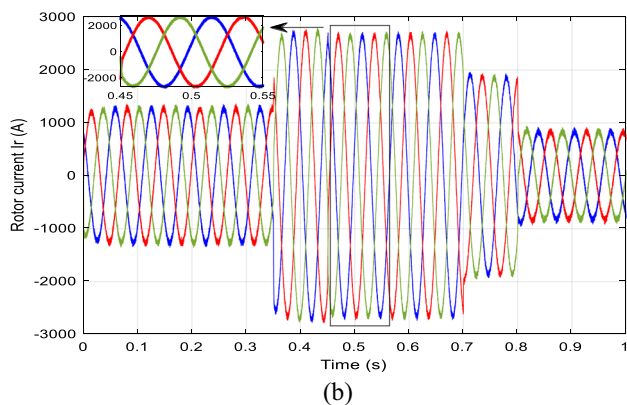
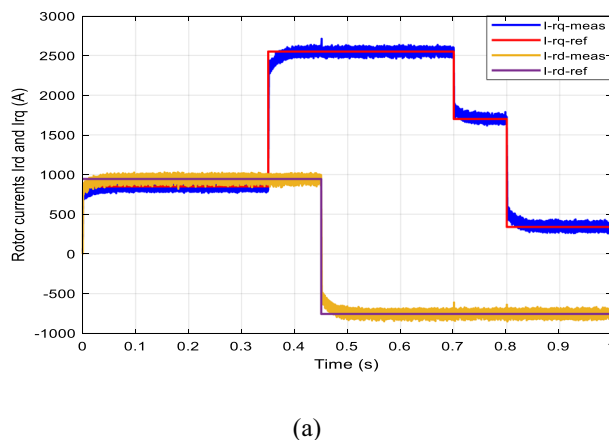


Fig. 5 Response of rotor current for power reference changes: a synchronous reference frame and b stationary reference frame

among the expected currents in Eqs. (30), (31), and their references. Equation (34) defines the function of cost.

$$F_j = \left(\begin{matrix} \Delta i_{dr_j}(k+1)^2 + \Delta i_{qr_j}(k+1)^2 + \\ \Delta i_{dg_j}(k+1)^2 + \Delta i_{qg_j}(k+1)^2 + i_m \end{matrix} \right) \quad (34)$$

where

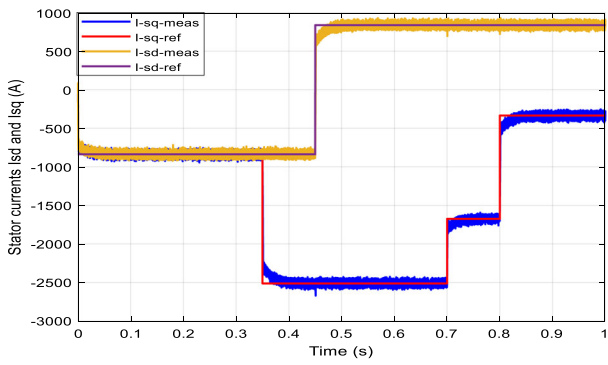
$$i_m = \begin{cases} \infty, & \text{if } |i_{k+1}| > |i_{max}| \\ 0, & \text{otherwise} \end{cases}, |i_{k+1}| = \sqrt{i_d(k+1)^2 + i_q(k+1)^2}$$

i_m represents DFIG and GSC overcurrent protection. The related voltage vector is disregarded if the current exceeds the limit value.

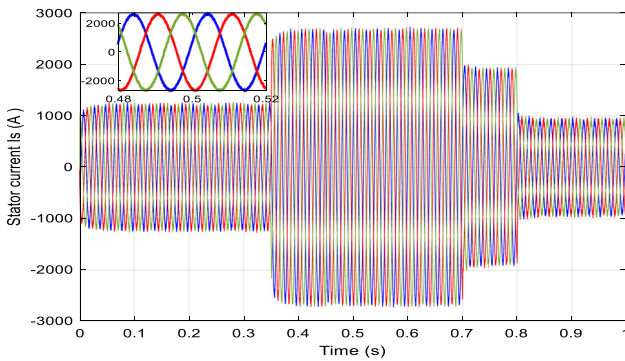
The application of an optimization process comes last. The ideal switching state combination $S_{DFIG(abc)}^{opt}$ and $S_{GSC(abc)}^{opt}$ that results in the lowest cost function is chosen $\min(F_j)$ in this process.

The model PC algorithm can be resumed as follows:

1. Feeding the GSC sampled reference rotor and current vector $i_{dq_r}^*, i_{dq_g}^*$, and the measured rotor and GSC current vector $i_{dq_r}(k), i_{dq_g}(k)$.



(a)



(b)

Fig. 6 Power reference-induced stator current response: a 2-phase frame and b 3-phase frame

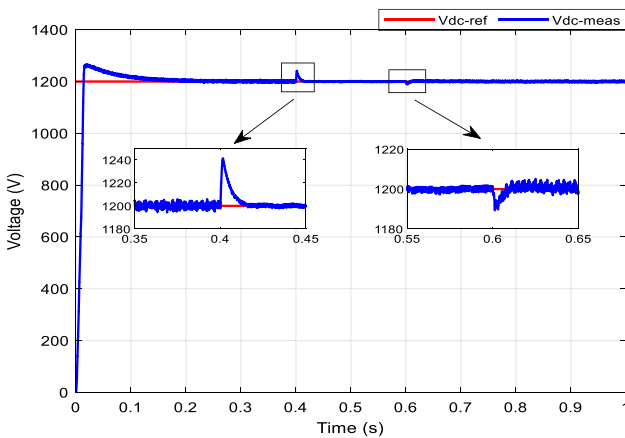
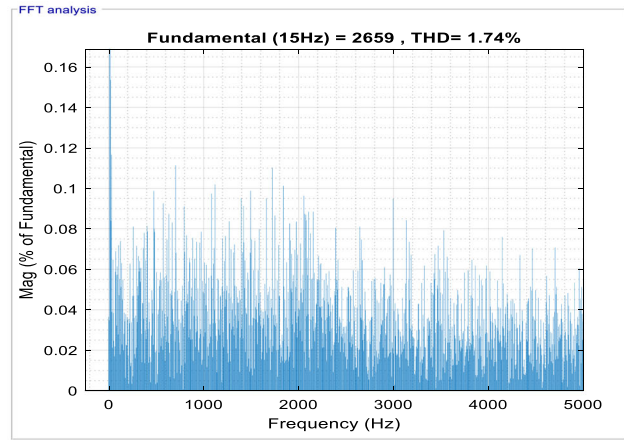
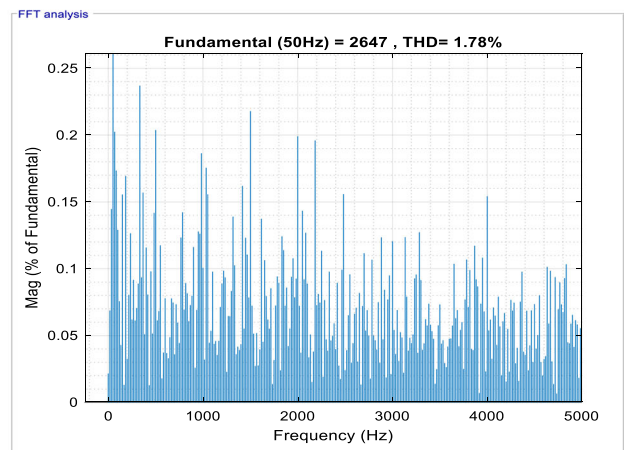


Fig. 7 The output voltage response of a GSC

2. Predict the current vector of the rotor and GSC $i_{dq_r_j}(k + 1)$, $i_{dq_g_j}(k + 1)$, using Eqs. (29) and (30) for every available commutation state. For a 3-phase 2-level voltage source converter, the commutation states (i.e., S_a , S_b , and S_c) can be derived from Eq. (34) and



(a)



(b)

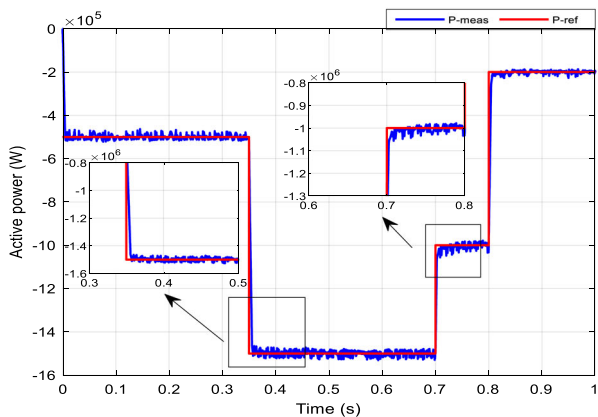
Fig. 8 THD value a rotor and b stator

Table 1.

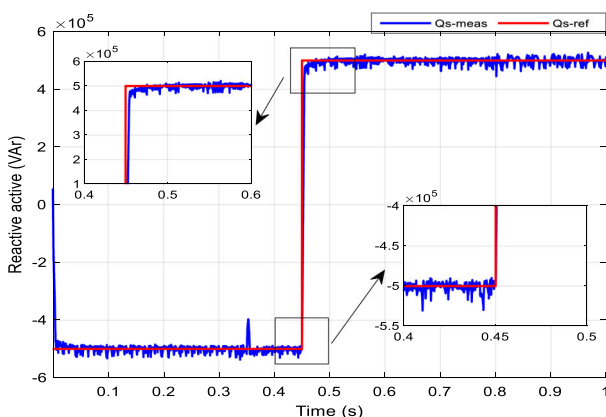
$$\bar{V} = \frac{2}{3} \bar{S}(x) \bar{A} \cdot V_{dc} \tag{35}$$

where $\bar{S}(x) = (S_a, S_b, S_c)$, $\bar{A} = \begin{pmatrix} 1 & e^{j(2\pi/3)} & e^{j(4\pi/3)} \end{pmatrix}$.

3. For each predicted current value, evaluate the cost function by using Eq. (34)
4. The loop will repeat until all voltage vectors have been validated in the cost function.
5. Select the switching state $S_{DFIG(abc)}^{opt}$ and $S_{GSC(abc)}^{opt}$ where the function of cost Eq. (34) is minimized (F_j^{opt}).



(a)



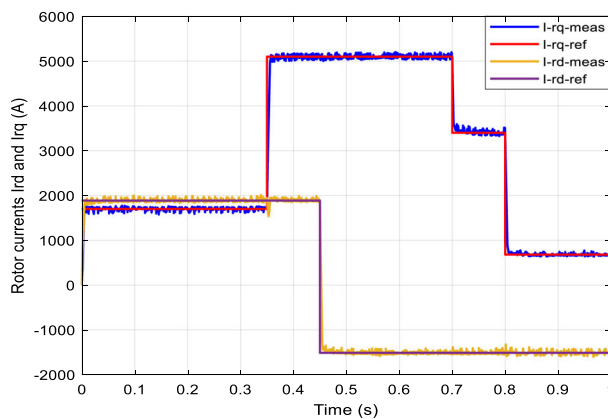
(b)

Fig. 9 Step change response in power references

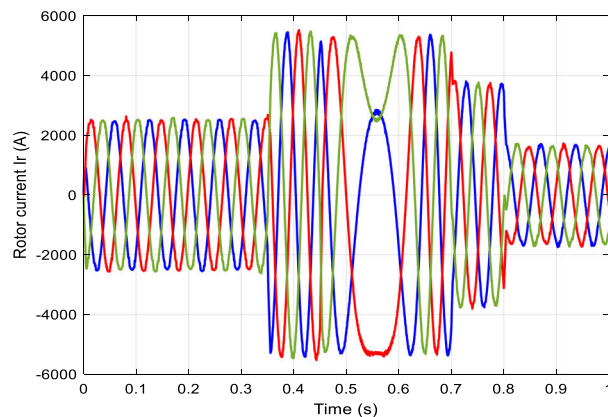
4 Results

The 1.5 MW DFIG suggested control is examined through simulation in this part using the MATLAB/SIMULINK software. The WES parameters we have worked with in our paper are given in Appendix. The sampling time is fixed at 10^{-4} s. Several simulation experiments were conducted to control the P_s and Q_s of the DFIG's stator side and filter them through its RSC and GSC.

A plan is designed to evaluate the proposed modified VC technique using robust model predictive rotor current control using a set of tests that ensure the efficiency of this control. A d -axis and a q -axis control, respectively, both the P_s and Q_s in this proposed system. Each controller has two loops—an external power loop and an internal current loop. With finite state space, the outputs of the inner loop controllers are restricted to $[318.2 \text{ V}; -318.2 \text{ V}]$. The values $K_P = 0.66 \times 75.75e - 1$ and $K_I = 0.66 \times 5354.55e - 1$ were chosen for the outer loop of the d and q -axis regulators, while the inner loop for both regulators is based on the proposed control FS-MPC.



(a)



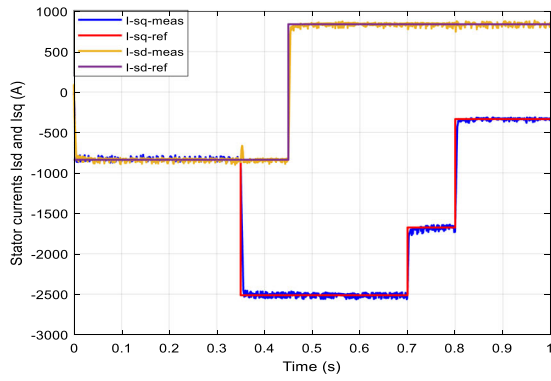
(b)

Fig. 10 Power reference-induced rotor current response: a 2-phase frame and b 3-phase frame

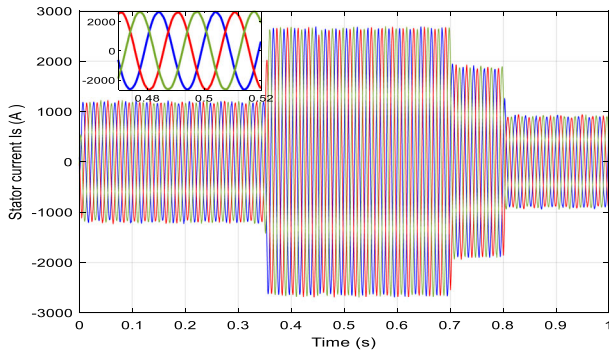
As for the GSC controller, the q -axis has two loops. At the same time, the d -axis has only an inner loop. So, the indoor unit is controlled by FS-MPC, where $k_p = 0.2$ and $k_i = 2.5$ parameters of the external d -axis controller that contribute to the continuous bus control. Moreover, since the FS-MPC technique uses the gate signal of the outer loop switches directly as control inputs, our paper's work is derived from this scheme's idea.

To examine the efficiency of the modified vector using robust model predictive rotor current control for various operating situations, the wind system underwent four distinct types of testing:

1. References tracking test (Figs. 4, 5, 6, 7, and 8).
2. Testing the robustness regarding the DFIG parameters variations (Figs. 9, 10, 11, and 12).
3. Inter-phase short-circuit faults test (reliability test).
4. Low-voltage transition testing (LVRT) (reliability test).



(a)



(b)

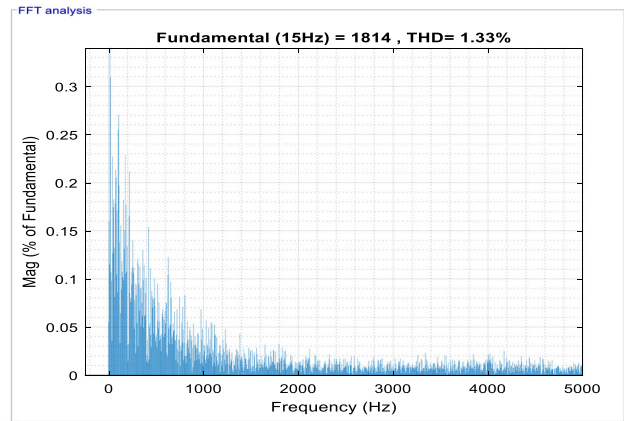
Fig. 11 Stator current’s reaction to changes in power references: **a** 2-phase frame and **b** 3-phase frame

4.1 Tracking Performance Test

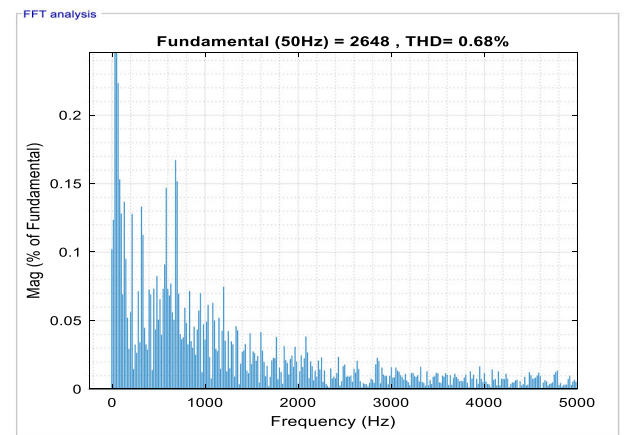
This section evaluated the modified vector using a robust model predictive rotor current control power tracking performance. DFIG and GSC have six and 4-time steps for prediction and control, respectively.

The tracking is tested for each power step. Firstly, the rotor mechanical speed is kept at $\Omega_m = 104.7$ rad/s to dispense with some factors that may affect the integrity of this test. P_{ref} is set to -0.5 MW for this test, with a power factor fixed to 0.69. Therefore, the Q_s setpoint Q_{ref} is -0.5 MVAR, which remains constant for 0.45 s. At 0.35 s, P_{ref} changes from -0.5 to -1.5 MW, and PF increases to 0.95.

Similarly, Q_{ref} takes a value of 0.5 MVAR at 0.45 s to show how controllable the P_s and Q_s decoupling is. At 0.7 s, P_{ref} goes from -1.5 to -1 MW, and the PF goes to 0.89. Consequently, Q_{ref} is maintained at its value of 0.5 MVAR. To reach 0.7 s, the power factor decreases to the value of 0.36, refer to the modification of the P_s reference value from 1 to 0.2 MW while keeping the Q_s reference at its former value (Fig. 4a and b).



(a)



(b)

Fig. 12 THD value: **a** rotor current and **b** stator current

For GSC control, the voltage reference is enforced equal to 1200 V (Fig. 7) and the reactive power reference equal to 80 KVAR, 0 KVAR value is enforced till 0.4 s, and this is due to control target (power factor equal to 1), then its value changes from 0 VAR to 50 KVAR starting from 0.6 s to demonstrate the separation between P_s , Q_s , and voltage value (Fig. 4c).

The THD of the DFIG stator and rotor current is calculated using FFT technique to prove the effectiveness of the proposed control to enhance the power quality, as presented in Fig. 8.

The system responses to these stepped changes are shown in Figs. 4, 5, 6, and 7. The response steps of P_s and Q_s are shown in Fig. 4. This figure shows that the MV-FS-MPC technique produces strong tracking performance with good P_s/Q_s separation. The zoomed-in figure shows that the MV-FS-MPC technique provides a faster response and reduced overshoot. The steady-state tracking performances are also acceptable at this time. It can be seen in the zoomed-in figure

Table 2 The values of the ripples in tracking test

	P_s (W)	Q_s (VAR)	I_{rq} (A)	I_{rd} (A)	I_{sq} (A)	I_{sd} (A)
Values	84,940	68,646	149.03	125.79	150.70	126.8

Table 3 The values of the ripples in robustness test

	P_s (W)	Q_s (VAR)	I_{rq} (A)	I_{rd} (A)	I_{sq} (A)	I_{sd} (A)
Tracking test	84,940	68,646	149.03	125.79	150.70	126.8
Robustness test	44,307	45,787.6	107	109	77	78
Ratios	48%	33%	28%	13%	49%	38%

Table 4 Percentage change in the THD value in the first and second tests

	THD value	
	Stator current	Rotor current
First test	1.78	1.74
Second test	0.68	1.33
THDR _{S1S2} (%)	61.79	23.56

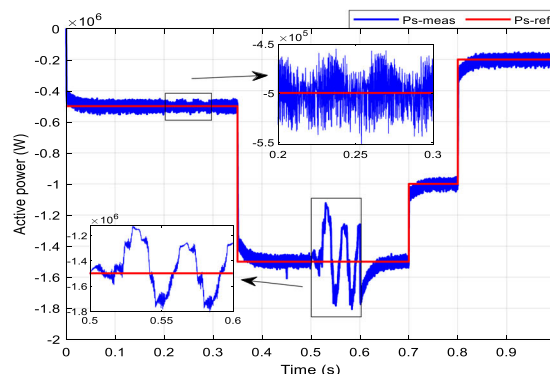
that the power output of the MV-FCS-MPC technique is considerably smoother, with fewer ripples in the P_s and Q_s .

The step response of the current in the stator and rotor is presented in Figs. 5 and 6. The step-wise dynamic responses of the rotor and stator currents are less than 50 ms. Figures 5a and 6a show that the rotor and stator currents exhibit excellent tracking performances compared to the predicted reference trajectories using the proposed MV-FS-MPC technique. As can be seen in the zoomed-in figure, the MV-FS-MPC technique has a significantly lower current ripple but a smaller overshoot and an acceptable dynamic response. This can immediately lead to lower torque ripple, reducing unit fatigue and associated maintenance costs.

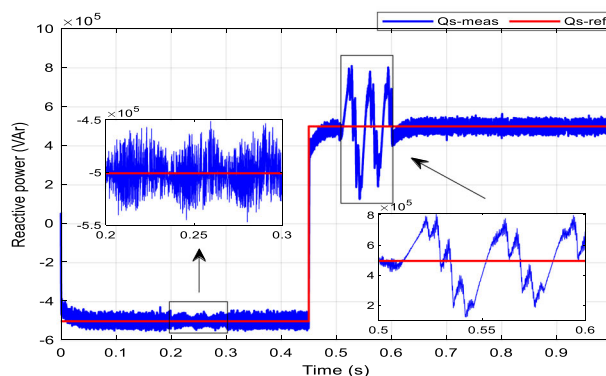
Figure 7 clearly shows the extent of the proposed control ability to impose a constant DC current value at 1200 V despite the change in reactive power references, as shown in the zoomed-in figure.

Further experiments showing the THD of the DFIG using the FFT approach for the MV-FS-MPC technique are given in Fig. 8. The THD of the stator current is estimated to be 1.78%. The THD of the rotor current is also predicted to be 1.74%.

Table 2 displays the output power and currents ripple values for the DFIG, serving as a reference for the comparative analysis of tests. It is noted from this table that the power and current ripples have significant values, which proves that the power quality is low and the same is true for current.



(a)

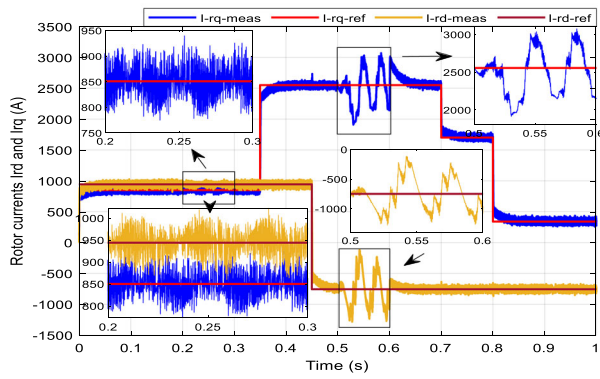


(b)

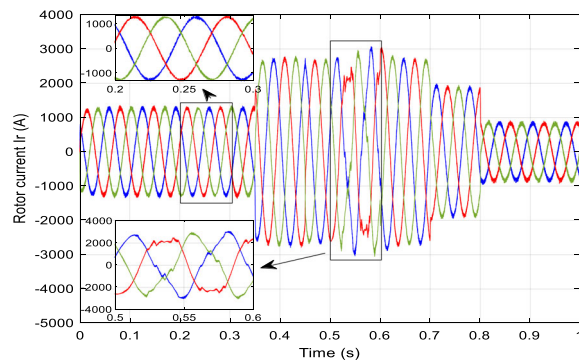
Fig. 13 Step change response in power references

4.2 Robustness Test

Second, the actual WS in a wind farm is always different due to the unpredictable nature of the environment. Depending on the actual WSs, the mechanical speed of the rotor must be adjusted. Otherwise, due to the slow response time of the pitch control system, the DFIG frequency output cannot be synchronized on the grid under different WSs. Therefore, the tracking performances (response time, overshoot, static error) for different power steps are examined while varying



(a)



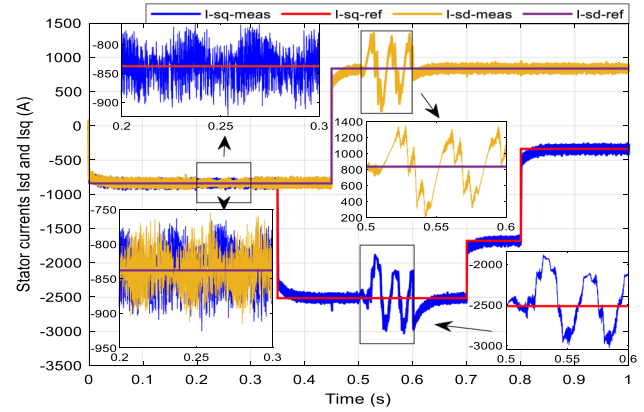
(b)

Fig. 14 Response of rotor current with the variation of the power references: **a** d-q frame and **b** a-b-c frame

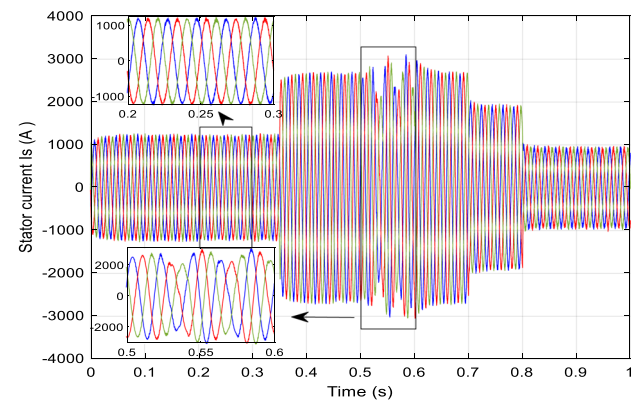
the mechanical speed of the rotor. To test the suggested MV-FS-MPC method, the rotor speed is increased from 104.7 to 209.45 rad/s throughout 0.3 to 0.6 s.

In addition, to assess the resilience of the MV-FS-MPC technique of the DFIG, we also examined how the parametric changes of the DFIG affected its performance. For this test, we heart the rotor windings to 100% of their rated value by increasing the rotor resistance (R_r), and we reduce the mutual inductance (L_m) to 30% of the rated value (the case of inductance saturation). The responses of the P_s (4 different steps with a negative sign to ensure delivery of energy to the electrical grid), Q_s (2 different steps to ensure decoupling between P_s and Q_s), rotor (to observe the effect of the speed change on the proposed control), and stator (quality of energy) current of the DFIG are presented in Figs. 9, 10, and 11, along with the simulation outcomes of this test, where the wind turbine operates from a -30 synchronous speed (104.7 rad/s) to a $+30$ synchronous speed (209.45 rad/s) before reaching 150 rad/s (synchronous speed).

Despite this test, the proposed control should give very satisfactory results in power quality. To confirm this, the THD value is measured at the stator (Fig. 12b) and rotor (Fig. 12a) current of the DFIG.



(a)



(b)

Fig. 15 Response of stator current with the variation of the power references: **a** d-q frame and **b** a-b-c frame

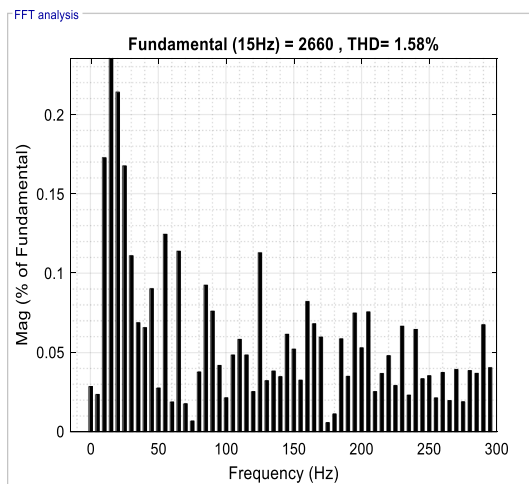
Figures 9 through 11 display the test findings. These findings demonstrate that the proposed MV-FS-MPC technique still offers adequate tracking performance about the specified reference trajectories for a range of rotor speeds and parameter variations. The suggested MV-FS-MPC technique still delivers a quicker reaction and a minor bypass than the first test. Better static tracking performance and comparable dynamic performance are both shown by MV-FS-MPC technique.

Figure 12 demonstrates the effectiveness of the suggested control, where the value of the THD of stator current is 0.68%, and the control gave a value of 1.33% for the THD value of the rotor current of the DFIG.

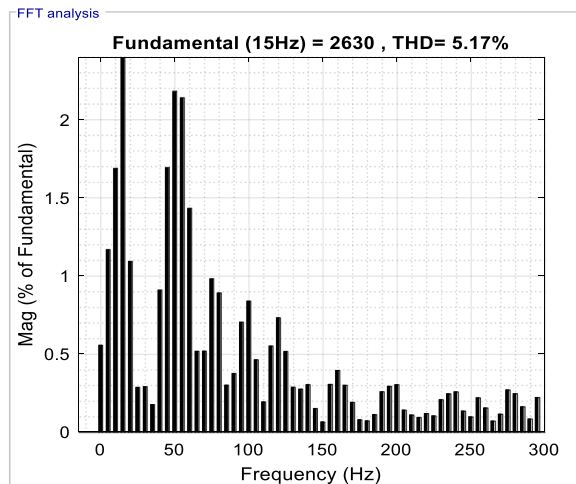
The numerical values of ripples at the level of P_s and Q_s and rotor and stator current with the d-q frame for the robustness test are listed in Table 3, where the reduction ratios were about 48%, 33%, 28%, 13%, 49%, and 38% for P_s , Q_s , I_{rq} , I_{rd} , I_{sq} , and I_{sd} , respectively, compared to the tracking test. So it can be said that the MV-FS-MPC technique is better in terms of reducing the value of the ripples in the robustness

Table 5 The values of the ripples in inter-phase short-circuit faults test

		P_s (W)	Q_s (VAR)	I_{rq} (A)	I_{rd} (A)	I_{sq} (A)	I_{sd} (A)
Tracking test		84,940	68,646	149.03	125.79	150.70	126.8
Short-circuit faults test	Fault No. 1	96,741.5	73,508.9	151	128	154.18	128
	Fault No. 2	427,623.8	546,391.2	737.21	948.5	725.55	934.65
Ratios	Fault No. 1	14%	7%	1%	2%	2%	1%
	Fault No. 2	77%	87%	80%	87%	79%	86%

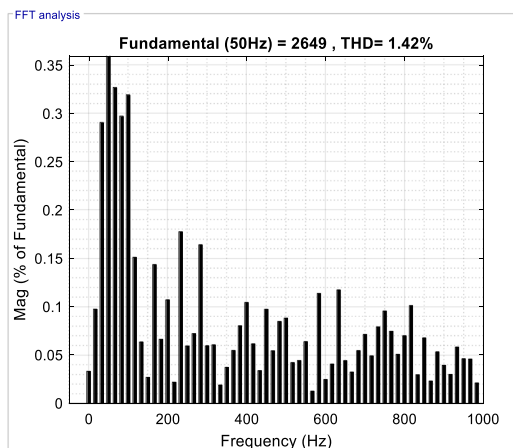


(a)

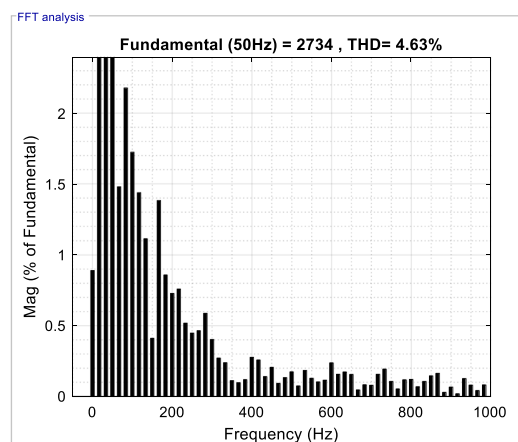


(b)

Fig. 16 THD values of the rotor current: **a** Fault No. 1 and **b** Fault No. 2



(a)



(b)

Fig. 17 THD values of the stator current: **a** Fault No. 1 and **b** Fault No. 2

Table 6 Values and ratios of the fundamental signal amplitude and THD of current in the different faults

	THD value		Fundamental signal amplitude (A)	
	Stator current (%)	Rotor current (%)	Stator current	Rotor current
Fault No. 1	1.42	1.58	2649	2660
Fault No. 2	4.63	5.17	2734	2630
Ratios (%)	69.33	69.43	3.10%	- 1.12%

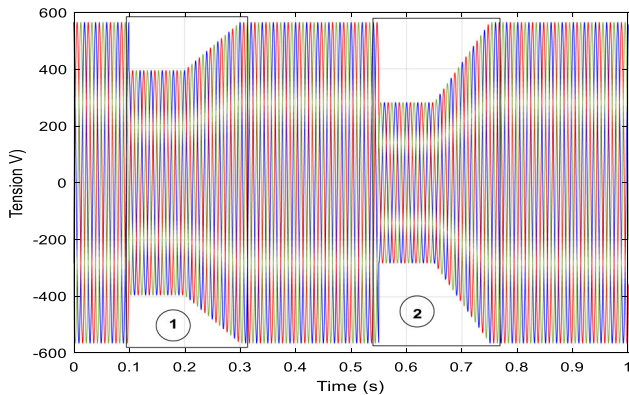


Fig. 18 The voltage grid dip

test; this is due to the control’s reliance on predicting currents based on the DFIG parameter.

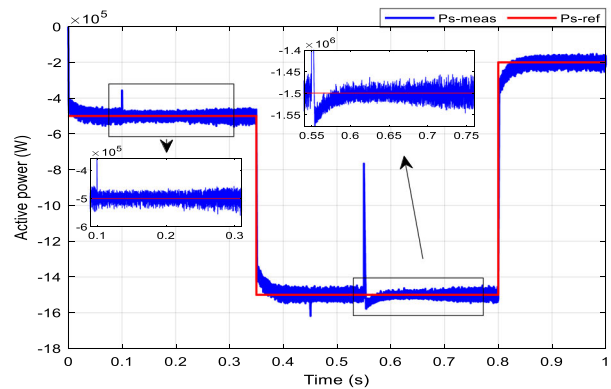
In Table 4, the percentage change in the value of THD of current between the first and second tests is calculated, where the percentage change is calculated according to Eq. (36). From this table, it is noted that the proposed strategy reduced the THD value of stator and rotor currents in the second test by an estimated percentage of 61.79% and 23.56%, respectively, compared to the second test, which indicates that the proposed strategy has a distinctive and effective performance if the system parameters are changed.

$$THDR_{S1S2}(\%) = \frac{THD_{S1} - THD_{S2}}{THD_{S1}} \quad (36)$$

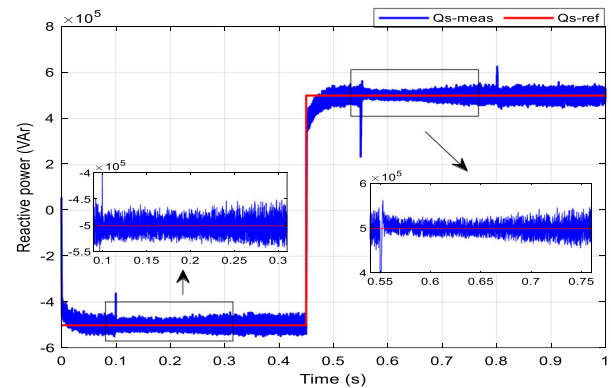
4.3 Inter-Phase Short-Circuit Faults Test

In this part, the proposed control ability is tested for excellent power control despite a fault at the level of the three phases of the RSC (circuit shortening). To prove the control power, a fault is imposed from 0.2 to 0.3 s in the first phase. Reaching 0.5 s, a fault occurs in the second and third phases at the same time. Through this proposed test, we obtained the results shown in Figs. 13, 14, and 15.

Figures 14 and 15 clearly show that a fault occurred at the level of the three phases in the two-time ranges from 0.2 to 0.3 s and from 0.5 to 0.6 s. In confirmation by Figs. 13,



(a)



(b)

Fig. 19 Step changes response in the power references

14a, and 15a, we note that the first fault does not affect the suggested control. While in the occurrence of the second fault, it is shown to what extent the control is affected by tracking the power and current references. In light of this effect, it cannot be said that the control is out of rule, but rather the presence of tracking with ripples in power and currents. From this, the proposed control has succeeded somewhat in the test. With its success, it is only proof of its efficiency.

Table 5 provides numerical values for ripples in P_s and Q_s , as well as rotor and stator current with the d-q frame. In comparison to the tracking test, the increase ratios were

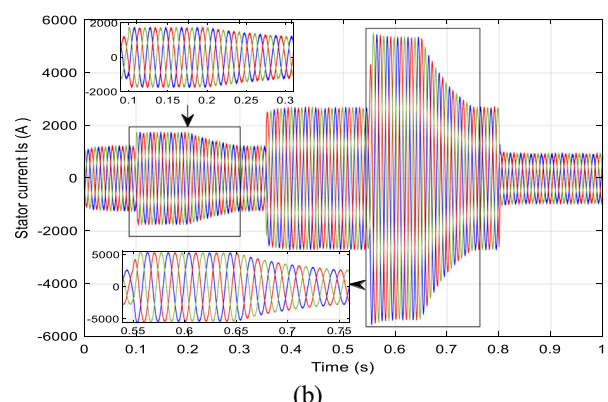
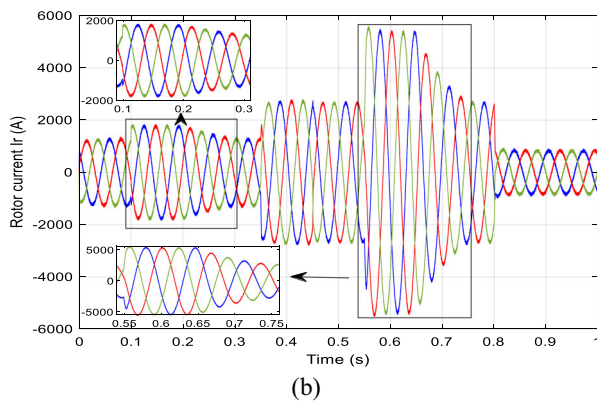
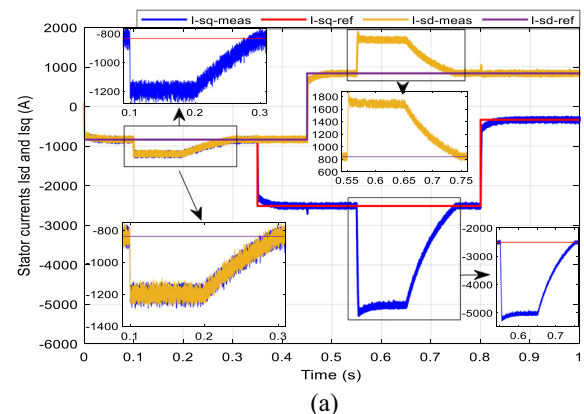
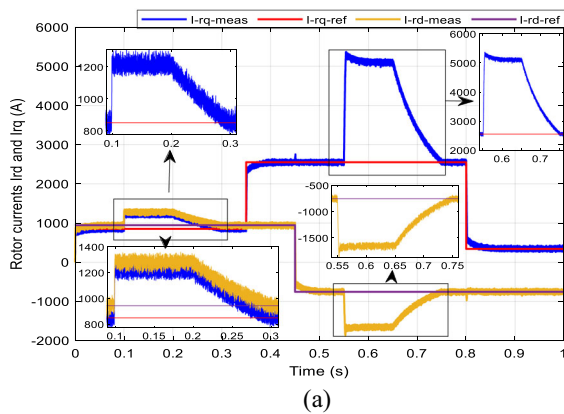


Fig. 20 The current response of the rotor to variations in power references: **a** 2-phase frame and **b** 3-phase frame

Fig. 21 The current response of the stator to variations in power references: **a** 2-phase frame and **b** 3-phase frame

approximately 14%, 7%, 1%, 2%, 2%, and 1% for P_s , Q_s , I_{rq} , I_{rd} , I_{sq} , and I_{sd} , respectively. Despite this modest increase resulting from the first fault, the control system remained unaffected, showcasing its efficiency and reliability.

The percentage increase in ripples due to the second fault, when compared to the ripple values of the first test, is estimated at 77%, 87%, 80%, 87%, 79%, and 86% for P_s , Q_s , I_{rq} , I_{rd} , I_{sq} , and I_{sd} , respectively. This substantial escalation underscores the significant impact of the second fault on the system. Nevertheless, the control system demonstrated remarkable resilience, maintaining convergence, stability, and tracking of its references throughout the occurrence of the fault.

By measuring the THD percentage (Figs. 16 and 17), it can be seen that the energy quality was not affected by the first fault ($THD_{rotor} = 1.58\%$ and $THD = 1.42\%$). As for fault No. 2, it can be observed that the energy quality deteriorates ($THD_{rotor} = 5.17\%$ and $THD_{stator} = 4.63\%$), but this value is acceptable compared to the first and second tests. This indicates the reliability and efficiency of the proposed control.

THD values for currents at faults No. 1 and No. 2 are represented in Figs. 16 and 17. The reduction ratios of the

THD of currents and signal amplitude value of fundamental (50 Hz) of currents are listed in Table 6. From this table, it is observed that the value of THD of stator current is low at fault No. 1. Compared to fault No. 2, the reduction percentage is estimated at 69.33%. The same applies to the rotor current, where the reduction ratio is estimated at 69.43%. In the case of static current, the value of fundamental amplitude is higher at fault No. 2 compared to fault No. 1, where the lift ratio is estimated at 3.10%. In the case of rotor current, the value of the amplitude of the fundamental signal is higher in the case of fault No. 1 compared to fault No. 2, where this increase is estimated at a rate of 1.12%.

4.4 Low-Voltage Ride-Through Testing

We test the LVRT of the MV-FS-MPC system. For this test, it is assumed that drop No. 1 occurs at 0.1 s and is filtered at 0.3 s. The grid voltage during the fault is eliminated by 30% compared to the nominal value. Drop No. 2 occurred in 0.55 s and was eliminated in 0.75 s. The stator voltage is eliminated by 50% compared to the nominal value during the fault. The velocity of the rotor is fixed at $\omega_m = 104.7$ rad/s, and the P_s and Q_s references of the stator are set at $P_{ref} =$

Table 7 The values of the ripples in LVRT testing

		P_s (W)	Q_s (VAR)	I_{rq} (A)	I_{rd} (A)	I_{sq} (A)	I_{sd} (A)
Tracking test		84,940	68,646	149.03	125.79	150.70	126.8
Short-circuit faults test	Drop 1	60,000	67,528	163.47	167	157	164
	Drop 2	50,292	48,312.1	183	168	180	167
Ratios	Drop 1	29%	1%	9%	25%	5%	23%
	Drop 2	40%	30%	19%	25%	17%	24%

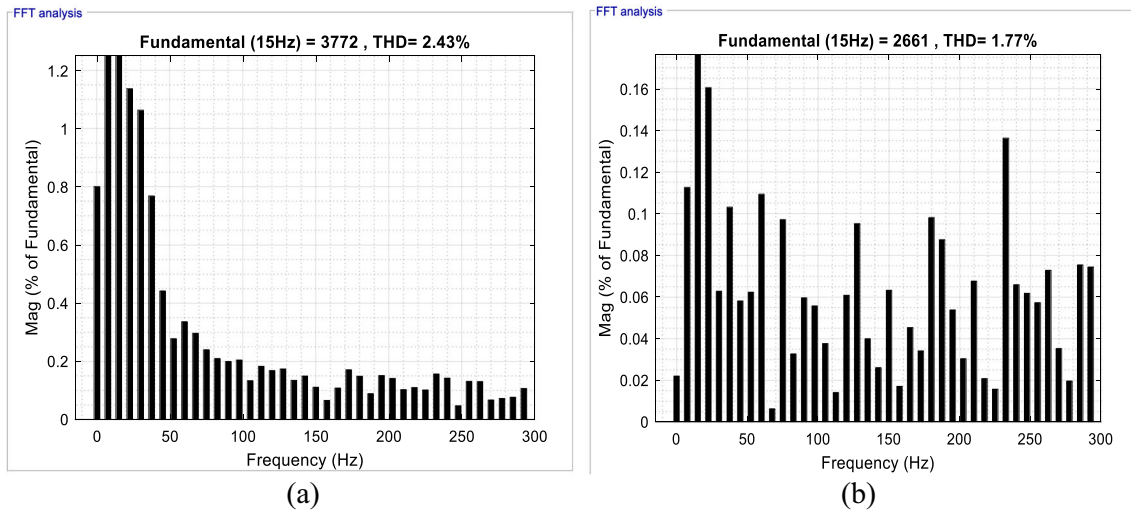


Fig. 22 THD values of the rotor current: **a** Drop No. 1 and **b** Drop No. 2

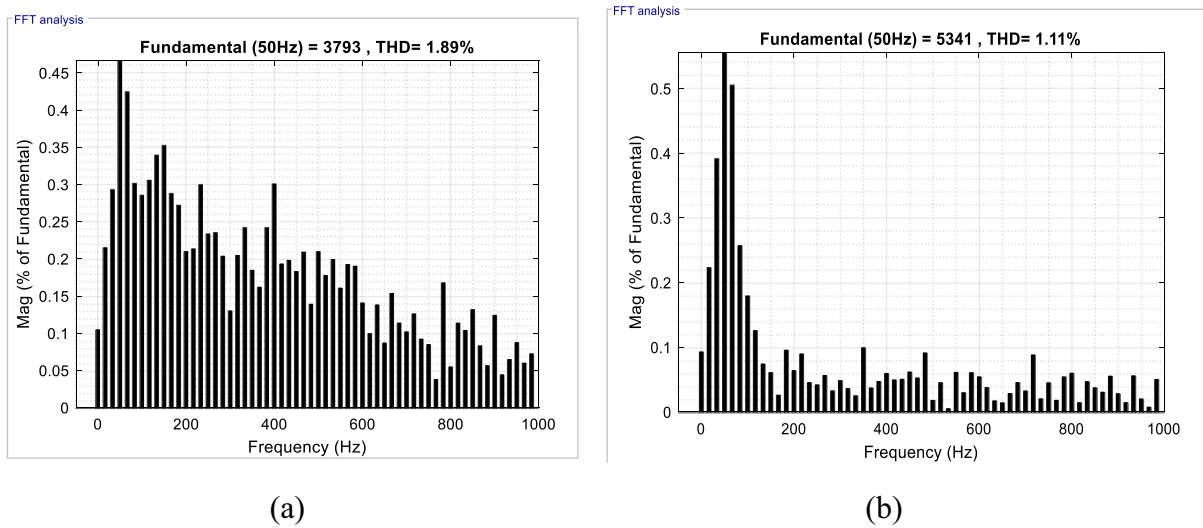


Fig. 23 THD values of the stator current: **a** Drop No. 1 and **b** Drop No. 2

Table 8 Ratios and values of the THD and fundamental signal amplitude in the different Drops

	THD value		Fundamental signal amplitude (A)	
	Stator current	Rotor current	Stator current	Rotor current
Drop No. 1	1.89	2.43	3793	3772
Drop No. 2	1.11	1.77	5341	2661
Ratios (%)	41.26%	27.16%	28.98	– 29.45

Table 9 Comparison of the command proposed in this paper with others in the literature

Tests Publication paper	Performance	Performance				Power quality THD%	Reliability	Robust
		Stability	Precision (%)	Rapidity RT (s)	Overshoot (%)			
[28]	B_SMC	Yes	0.09	0.03	–	0.89	–	–
[77]	FOC	Yes	–	0.09	–	5.17	–	–
	DPC	Yes	–	0.02	–	5.95	–	–
[3]	Backstepping	Yes	–	–	–	0.31	–	–
[79, 81]	DTC	Yes	–	0.12	–	18.8	–	–
	FCS	Yes	–	0.16	–	8.26	–	–
	MPDC	Yes	–	0.15	–	8.17	–	–
[45, 81]	FCS-MPC	Yes	–	0.15	–	6.12	–	–
[80]	FCS-MPC	Yes	0.4	0.4	–	0.29	–	–
[81]	FCS-MPC	Yes	0.11	0.11	–	0.49	–	–
[49]	FCS-MPC	Yes	–	–	–	8.82	–	–
	Dead-beat-PC					4.49		
[82]	FCS-MPC	Yes	0.4	0.02	0.03	0.32	Yes	Yes
[83]	IBC	Yes	–	0.0285	0.001	6.04	Yes	Yes
Proposed technique	VM-FS-MPC	Yes	0.069	0.0497	0.02559	1.7	Yes	Yes

– 0.5 MW and then at 0.35 s, $P_{ref} = -1.5$ MW until 0.8 s, $P_{ref} = -0.2$ MW and $Q_{ref} = -0.5$ MVAR continues until 0.45 s to become $Q_{ref} = 0.5$ MVAR, respectively (Figs. 18, 19, 20 and 21).

The Danish grid code was the basis for the dip utilized in our study [76]. The voltage dip characteristics (Fig. 18):

- Symmetrical 3-phase voltage drop.
- 30%, then a 50% drop at the nominal voltage for 0.1 s.
- The linear increase in voltage to the nominal voltage throughout 0.1 s.

The results obtained in Figs. 18, 19, 20, and 21 show that drop No. 1 has significantly lower overshooting and slightly improved tracking performances than drop No. 2. The excesses given by the proposed controller resulting from drop No. 2 are almost tolerable compared to the high drop ratio. However, the ripple of power and currents compared to the third test results in both cases is almost nonexistent. This

comparison shows that the suggested MV-FS-MPC method significantly improves LVRT performance by successfully reducing the excess current caused by grid disturbance.

Table 7 highlights noticeable fluctuations in ripple ratios for power and currents, ranging from 1 to 40% compared to the values observed in the first test. Remarkably, these variations are within acceptable limits, demonstrating the effective performance of the control system in maintaining stability even amid sudden drops. Despite the observed drops, Figs. 22 and 23 visually depict that the proposed control remains reliable, effectively preserving the quality of extracted energy.

In Table 8, the ratios and values of the THD and fundamental signal amplitude in the different Drops are shown. This table is filled out using Figs. 22 and 23. From this table, it is noted that the THD value for streams is low at Drop No. 2 compared to Drop No.1, which was reduced by an estimated percentage of 41.26% and 27.16% for both stator and rotor current, respectively. As for the amplitude of the fundamental signal (50 Hz) of the stator current, it is higher in Drop

No. 2 compared to Drop No. 1, as the percentage increase in amplitude is estimated at 28.98% compared to Drop No. 1. But with regard to the rotor current, it is noted that the amplitude of the fundamental signal of the rotor current is lower in Drop No. 2 compared to Drop No. 1, where the reduction percentage is estimated at -29.45% compared to Drop No. 1.

Table 9 compares the proposed control with other research. The proposed method succeeded in testing robustness and reliability. MV-FS-MPC technique increases performance compared to [3, 28, 80–82], but its biggest benefit is the reduction of THD compared to [45, 49, 60, 77, 83], which did not exceed 1.7%, indicating superior power quality.

5 Conclusions

The power regulation of DFIG systems and GSC is discussed in this study using a completely new, time-efficient MV-FS-MPC technique. This technique analytically transforms the vector-PI robustness issue into a manageable FS problem, which can be addressed quickly. The proposed technique leads to good power tracking, robustness performances, and rapid running times, according to simulation findings. The comparison of the tests illustrates that the proposed scheme significantly reduces computation time while achieving good control performance in settling time, overshoot, error static, and rejection of perturbations, in addition to high energy quality. This suggests that the proposed scheme strikes a good balance between computational time and the performance of the control. Future work will involve synchronizing the converter side control of the rotor and the grid, taking into account additional situations, and improving the DFIG control performance by modifying the suggested MV-FS-MPC by replacing the pi controller with a backstepping approach (i.e., building a predictive-backstepping scheme), our paper may open the possibility of achieving this.

Appendix

See Tables 10, 11 and 12.

Table 10 DFIG parameters

P_n	1.5 MW
v	12.5 m/s
V_s	398/690 V
I_n	1900 A
f	50 Hz
L_s	0.0137 H
L_r	0.0136 H
M	0.0135 H
R_s	0.012 Ω
R_r	0.021 Ω
p	2
J	1000 kg m ²

Table 11 Wind turbine parameters

Number of blades	3
R	35.25 m
G	90
J	1000 kg m ²
f_v	0.0024 N ms ⁻¹
V_d	4 m/s
V_m	25 m/s

Table 12 Grid link settings

ω_s	$2\pi 50$ rad/s
R_g	2 m Ω
L_g	5 mH
C_{DC}	4400 μ F

Funding Open access funding provided by the Scientific and Technological Research Council of Türkiye (TÜBİTAK). The authors extend their appreciation to the Deanship of Scientific Research at King Khalid University under for funding this work through General Research Project under Grant number (RGP.2/33/45).

Data Availability Data are available on request from the authors. The datasets used and/or analyzed during the current study are available from the first author on reasonable request. In the event of communication, the first author (Abdelkader achar, E-mail: a.achar1@yahoo.com) will respond to any inquiry or request.

Declarations

Conflict of interest The authors declare that they no conflict of interest.

Ethical Approval Not applicable.

Informed Consent Not applicable.

Open Access This article is licensed under a Creative Commons Attribution 4.0 International License, which permits use, sharing, adaptation, distribution and reproduction in any medium or format, as long as you give appropriate credit to the original author(s) and the source, provide a link to the Creative Commons licence, and indicate if changes were made. The images or other third party material in this article are included in the article's Creative Commons licence, unless indicated otherwise in a credit line to the material. If material is not included in the article's Creative Commons licence and your intended use is not permitted by statutory regulation or exceeds the permitted use, you will need to obtain permission directly from the copyright holder. To view a copy of this licence, visit <http://creativecommons.org/licenses/by/4.0/>.

References

1. Ellabban, O.; Abu-Rub, H.; Blaabjerg, F.: Renewable energy resources: current status, future prospects and their enabling technology. *Renew. Sustain. Energy Rev.* **39**, 748–764 (2014)
2. Deploying Renewables 2011, (www.iae.org) [accessed on 15/8/2013].
3. Achar, A.; Djeriri, Y.; Bentaallah, A.; Hanafi, S.; Djehaf, M.A.; Bouddou, R.: Lyapunov-based robust power controllers for a wind farm using parallel multicell converters. *Przełąd Elektrotechniczny*. **99**(4), 247–254 (2023)
4. Benbouhenni, H.; Bizon, N.; Colak, I.; Thounthong, P.; Takorabet, N.: Simplified super twisting sliding mode approaches of the double-powered induction generator-based multi-rotor wind turbine system. *Sustainability* **14**, 5014 (2022). <https://doi.org/10.3390/su14095014>
5. Benbouhenni, H.; Boudjema, Z.; Bizon, N.; Thounthong, P.; Takorabet, N.: Direct power control based on modified sliding mode controller for a variable-speed multi-rotor wind turbine system using PWM strategy. *Energies* **15**, 3689 (2022). <https://doi.org/10.3390/en15103689>
6. Sara, K.; Khoukha, I.; El Madjid, B.; Benbouhenni, H.; Emad, A.: A direct vector control based on modified SMC theory to control the double-powered induction generator-based variable-speed contra-rotating wind turbine systems. *Energy Rep.* (2022). <https://doi.org/10.1016/j.egy.2022.11.052>
7. Habib, B.; Elhadj, B.; Hamza, G.; Nicu, B.; Ilhami, C.: A new PD(1+PI) direct power controller for the variable-speed multi-rotor wind power system driven doubly-fed asynchronous generator. *Energy Rep.* **8**, 15584–15594 (2022). <https://doi.org/10.1016/j.egy.2022.11.136>
8. Cai, C.; Jiang, B.; Deng, L.: General dynamic equivalent modeling of microgrid based on physical background. *Energies* **8**, 12929–12948 (2015). <https://doi.org/10.3390/en81112354>
9. Okedu, K.E.; Muyeen, S.M.: Comparative performance of DFIG and PMSG wind turbines during transient state in weak and strong grid conditions considering series dynamic braking resistor. *Energies* **15**, 9228 (2022). <https://doi.org/10.3390/en15239228>
10. Jung, S.; Yoo, Y.; Kim, H.; Lee, J.-H.; Yoon, M.; Jang, G.: Development of an active power reserve management method for DC applied wave-wind combined generation systems. *Energies* **8**, 12488–12504 (2015). <https://doi.org/10.3390/en81112321>
11. Sara, K.; Habib, B.; Emad, A.; Khoukha, I.; El Madjid, B.: Implementation of third-order sliding mode for power control and maximum power point tracking in DFIG-based wind energy systems. *Energy Rep.* **10**, 3561–3579 (2023). <https://doi.org/10.1016/j.egy.2023.09.187>
12. Errouissi, R.; Al-Durra, A.; Muyeen, S.M.; Leng, S.; Blaabjerg, F.: Offset-free direct power control of DFIG under continuous-time model predictive control. *IEEE Trans. Power Electron.* **32**(3), 2265–2277 (2016)
13. Zin, A.A.B.M.; Pesaran, H.A.M.; Khairuddin, A.B.; Jahanshaloo, L.; Shariati, O.: An overview on doubly fed induction generators' controls and contributions to wind based electricity generation. *Renew. Sustain. Energy Rev.* **27**, 692–708 (2013)
14. Cardoso, J.G.; Casella, I.R.S.; Sguarezzi Filho, A.J.; Costa, F.F.; Capovilla, C.E.: SCIG wind turbine wireless controlled using morphological filtering for power quality enhancement. *Renew. Energy* **92**, 303–311 (2016)
15. Benbouhenni, H.; Colak, I.; Bizon, N.; Mazare, A.G.; Thounthong, P.: Direct vector control using feedback PI controllers of a dpag supplied by a two-level PWM inverter for a multi-rotor wind turbine system. *Arab. J. Sci. Eng.* **48**(7), 15177–15193 (2023)
16. Xiahou, K.; Li, M.S.; Liu, Y.; Wu, Q.H.: Sensor fault tolerance enhancement of DFIG-WTs via perturbation observer-based DPC and two-stage Kalman filters. *IEEE Trans. Energy Convers.* **33**(2), 483–495 (2018)
17. Quan, Y.; Hang, L.; He, Y.; Zhang, Y.: Multi-resonant-based sliding mode control of DFIG-based wind system under unbalanced and harmonic network conditions. *Appl. Sci.* **9**, 1124 (2019)
18. El Ouanjli, N.; Aziz, D.; El Ghzizal, A.; Mohammed, T.; Youness, E.; Khalid, M.; Badre, B.: Direct torque control of doubly fed induction motor using three-level NPC inverter. *Protect. Contr. Modn. Power Syst.* **4**(17), 1–9 (2019)
19. Amrane, F.; Chaiba, A.; Babas, B.E.; Mekhilef, S.: Design and implementation of high performance field oriented control for grid-connected doubly fed induction generator via hysteresis rotor current controller. *Rev. Sci. Techni.-Electrotechn. Et Energ.* **61**(4), 319–324 (2016)
20. Habib, B.; Gasmı, H.; Colak, I.: Intelligent control scheme of asynchronous generator-based dual-rotor wind power system under different working conditions. *Majlesi J. Energy Manag.* **11**(3), 8–15 (2022)
21. Benbouhenni, H.; Bizon, N.: Terminal synergetic control for direct active and reactive powers in asynchronous generator-based dual-rotor wind power systems. *Electronics* **10**, 1880 (2021). <https://doi.org/10.3390/electronics10161880>
22. Bektache, A.; Boukhezzer, B.: Nonlinear predictive control of a DFIG-based wind turbine for power capture optimization. *Int. J. Electr. Power Energy Syst.* **101**, 92–102 (2018)
23. Han, Y.; Ma, R.: Adaptive-gain second-order sliding mode direct power control for wind-turbine-driven DFIG under balanced and unbalanced grid voltage. *Energies* **12**, 3886 (2019)
24. Benbouhenni, H.; Bizon, N.; Colak, I.; Thounthong, P.; Takorabet, N.: Application of fractional-order PI controllers and neuro-fuzzy



- PWM technique to multi-rotor wind turbine systems. *Electronics* **11**, 1340 (2022). <https://doi.org/10.3390/electronics11091340>
25. Habib, B.; Gasmi, H.; Colak, I.: Backstepping control for multi-rotor wind power systems. *Majlesi J. Energy Manag.* **11**(4), 8–15 (2022)
 26. Chojaa, H.; Derouich, A.; Chehaidia, S.E.; Zamzoum, O.; Taoussi, M.; Benbouhenni, H.; Mahfoud, S.: Enhancement of direct power control by using artificial neural network for a doubly fed induction generator-based WECS: an experimental validation. *Electronics* **11**, 4106 (2022). <https://doi.org/10.3390/electronics11244106>
 27. Yang, D.; Huang, X.; Yang, X.: A hybrid nonlinear active control strategy combining dry friction control and nonlinear velocity compensation control. *Appl. Sci.* **11**, 11670 (2021). <https://doi.org/10.3390/app112411670>
 28. Echiheb, F.; Ihedrane, Y.; Bossoufi, B., et al.: Robust sliding-Backstepping mode control of a wind system based on the DFIG generator. *Sci. Rep.* (2022). <https://doi.org/10.1038/s41598-022-15960-7>
 29. Benbouhenni, H.; Bizon, N.: A synergetic sliding mode controller applied to direct field-oriented control of induction generator-based variable speed dual-rotor wind turbines. *Energies* **14**, 4437 (2021). <https://doi.org/10.3390/en14154437>
 30. Benbouhenni, H.; Ilhami, C.; Nicu, B.; Emad, A.: Fractional-order neural control of a DFIG supplied by a two-level PWM inverter for dual-rotor wind turbine system. *Measur. Contr.* (2023). <https://doi.org/10.1177/00202940231201375>
 31. Benbouhenni, H.; Nicu, B.; Mohamed, I.M.; Ilhami, C.; Abdelkadir, B.D.; Hamza, G.: Enhancement of the power quality of DFIG-based dual-rotor wind turbine systems using fractional order fuzzy controller. *Exp. Syst. Appl.* **238**(12), 121695 (2024). <https://doi.org/10.1016/j.eswa.2023.121695>
 32. Habib, B.; Gasmi, H.; Colak, I.: Intelligent control scheme of asynchronous generator-based dual-rotor wind power system under different working conditions. *Majlesi Journal of Energy Management.* **11** (2022). <https://em.majlesi.info/index.php/em/article/view/494>.
 33. Habib, B.; Bizon, N.: A synergetic sliding mode controller applied to direct field-oriented control of induction generator-based variable speed dual-rotor wind turbines. *Energies* (2021). <https://doi.org/10.3390/en14154437>
 34. de Oliveira Filho, M.E.; Gazoli, J.R.; Sguarezi Filho, A.J.; Ruppert Filho, E.: 2008 A control method for voltage source inverter without dc link capacitor. In: *IEEE Power electronics specialists conference*. pp. 4432–4437 (2008).
 35. Benbouhenni, H.; Boudjema, Z.; Belaidi, A.: DFIG-based wind turbine system using four-level FSVM strategy. *Majlesi J. Energy Manag.* **6**(3), 7–19 (2017)
 36. Benbouhenni, H.; Boudjema, Z.; Belaidi, A.; A.: DFIG-based WT system using FPWM inverter. *Int. J. Smart Grid.* **2**(3), 142–154 (2018)
 37. Benbouhenni, H.: Comparative study between different vector control methods applied to DFIG wind turbines. *Majlesi J. Mechatr. Syst.* **7**(4), 15–23 (2018)
 38. Benbouhenni, H.: Stator active and reactive power ripples minimization for DVC control of DFIG by using five-level neural space vector modulation. *Acta Electrotechnica et Informatica.* **2**, 16–23 (2019)
 39. Mishra, Y.; Mishra, S.; Tripathy, M.; Senroy, N.; Dong, Z.Y.: Improving stability of a DFIG-based wind power system with tuned damping controller. *IEEE Trans. Energy Convers.* **24**(3), 650–660 (2009)
 40. Tang, Y.; Ju, P.; He, H.; Qin, C.; Wu, F.: Optimized control of DFIG-based wind generation using sensitivity analysis and particle swarm optimization. *IEEE Trans. Smart Grid.* **4**(1), 509–520 (2013)
 41. Tummala, A.S.; Alluri, H.K.; Ramanarao, P.V.: Optimal control of DFIG wind energy system in multi-machine power system using advanced differential evolution. *IETE J. Res.* **66**(1), 91–102 (2020)
 42. Ayyarao, T.S.: Modified vector controlled DFIG wind energy system based on barrier function adaptive sliding mode control. *Protect. Control Modn Power Syst.* **4**(1), 1–8 (2019)
 43. Ahmed, H.M.; Jlassi, I.; Cardoso, A.J.M.; Bentaallah, A.: Model-free predictive current control of synchronous reluctance motors based on a recurrent neural network. *IEEE Trans. Industr. Electron.* **69**(11), 10984–10992 (2021)
 44. Lunardi, A.; Sguarezi Filho, A.J.: Current control for DFIG systems under distorted voltage using predictive–repetitive control. *IEEE J. Emerg. Select. Topics Power Electr.* **9**(4), 4354–4363 (2020)
 45. Kou, P.; Liang, D.; Li, J.; Gao, L.; Ze, Q.: Finite-control-set model predictive control for DFIG wind turbines. *IEEE Trans. Autom. Sci. Eng.* **15**(3), 1004–1013 (2017)
 46. Rodrigues, L.L.; Vilcanqui, O.A.; Murari, A.L.; Sguarezi Filho, A.J.: Predictive power control for DFIG: A FARE-based weighting matrices approach. *IEEE J. Emerg. Select. Topics Power Electr.* **7**(2), 967–975 (2019)
 47. Gontijo, G.F.; Tricarico, T.C.; França, B.W.; Da Silva, L.F.; Van Emmerik, E.L.; Aredes, M.: Robust model predictive rotor current control of a DFIG connected to a distorted and unbalanced grid driven by a direct matrix converter. *IEEE Trans. Sustain. Energy* **10**(3), 1380–1392 (2018)
 48. Kumar, R.; Das, S.; Bhaumik, A.: Speed sensorless model predictive current control of doubly-fed induction machine drive using model reference adaptive system. *ISA Trans.* **86**, 215–226 (2019)
 49. Hassine, I.M.B.; Naouar, M.W.; Mrabet-Bellaaj, N.: Predictive control strategies for wind turbine system based on permanent magnet synchronous generator. *ISA Trans.* **62**, 73–80 (2016)
 50. Benbouhenni, H.; Bizon, N.: Third-order sliding mode applied to the direct field-oriented control of the asynchronous generator for variable-speed contra-rotating wind turbine generation systems. *Energies* **14**, 5877 (2021)
 51. Kadi, S.; Khoukha, I.; El Madjid, B.; Benbouhenni, H.; Emad, A.: A direct vector control based on modified SMC theory to control the double-powered induction generator-based variable-speed contra-rotating wind turbine systems. *Energy Rep.* **8**, 15057–15066 (2022)
 52. Benbouhenni, H.; Lemdani, S.: Combining synergetic control and super twisting algorithm to reduce the active power undulations of doubly fed induction generator for dual-rotor wind turbine system. *Electr. Eng. Electromech.* **3**, 8–17 (2021)
 53. Benbouhenni, H.; Driss, A.; Lemdani, S.: Indirect active and reactive powers control of doubly fed induction generator fed by three-level adaptive-network-based fuzzy inference system – pulse width modulation converter with a robust method based on super twisting algorithms. *Electr. Eng. Electromech.* **4**, 8–17 (2021)
 54. Habib, B.; Bizon, N.: Advanced direct vector control method for optimizing the operation of a double-powered induction generator-based dual-rotor wind turbine system. *Mathematics* **9**, 2403 (2021)
 55. Habib, B.: Comparison study between seven-level SVPWM and two-level SVPWM strategy in direct vector control of a DFIG-based wind energy conversion systems. *Int. J. Appl. Power Eng. (IJAPE).* **9**(1), 12–21 (2020)
 56. Benbouhenni, H.; Boudjema, Z.; Belaidi, A.: DFIG-based wind energy conversion system using five-level FSVM technique. *Int. J. Renew. Energy Technol.* **11**(2), 147–164 (2020)
 57. Habib, B.: Direct vector control for doubly fed induction generator-based wind turbine system using five-level NSVM and two-level NSVM technique. *Int. J. Smart Grid.* **3**(1), 25–32 (2019)
 58. Benbouhenni, H.; Boudjema, Z.; Belaidi, A.; A.: Using three-level Fuzzy space vector modulation method to improve indirect vector control strategy of a DFIG based wind energy conversion systems. *Int. J. Smart Grid* **2**(3), 155–171 (2018)



59. Benbouhenni, H.; Boudjema, Z.; Belaidi, A.: Indirect vector control of a DFIG supplied by a two-level FSVM inverter for wind turbine system. *Majlesi J. Electr. Eng.* **13**(1), 45–54 (2019)
60. Benbouhenni, H.; Boudjema, Z.; Belaidi, A.; A.: Intelligent SVM technique of a multi-level inverter for a DFIG-based wind turbine system. *Int. J. Digital Signal Smart Syst.* **3**(123), 4–19 (2019)
61. Gasmı, H.; Mendaci, S.; Laifa, S.; Kantas, W.; Benbouhenni, H.: Fractional-order proportional-integral super twisting sliding mode controller for wind energy conversion system equipped with doubly fed induction generator. *J. Power Electron.* **22**(8), 1357–1373 (2022)
62. Gasmı, H.; Benbouhenni, H.; Mendaci, S.; Colak, I.: A new scheme of the fractional-order super twisting algorithm for asynchronous generator-based wind turbine. *Energy Rep.* **9**, 6311–6327 (2023)
63. Javadi, M.; Malyscheff, A.M.; Wu, D.; Kang, C.; Jiang, J.N.: An algorithm for practical power curve estimation of wind turbines. *CSEE J. Power Energy Syst.* **4**(1), 93–102 (2018)
64. Lin, W.; Wen, J.; Cheng, S.; Lee, W.J.: An investigation on the active power variations of wind farms. *IEEE Ind. Appl. Soci. Annual Meet.* **48**(3), 1087–1094 (2012). <https://doi.org/10.1109/TIA.2012.2190817>
65. Liu, X.; Kong, X.: Nonlinear model predictive control for DFIG-based wind power generation. *IEEE Trans. Autom. Sci. Eng.* **11**(4), 1046–1055 (2013)
66. Sguarezi Filho, A.J.; Ruppert Filho, E.: Model-based predictive control applied to the doubly-fed induction generator direct power control. *IEEE Trans. Sustain. Energy.* **3**(3), 398–406 (2012)
67. Dias, S.V.; Neto, T.R.; dos Reis, L.L.; Torrico, B.C.; Campos, J.C.T.: Robust analysis of a predictive controller of DFIG wind energy systems. In: *IEEE 8th international symposium on power electronics for distributed generation systems (PEDG)*. pp. 1–5 (2017).
68. Ouari, K.; Rekioua, T.; Ouhrouche, M.: Nonlinear model predictive controller of a variable speed wind turbine driven doubly fed induction generator. *J. Electr. Syst.* **9**(2), 243–255 (2013)
69. Lunardi, A.S.; Sguarezi Filho, A.J.: Controle preditivo baseado em modelo para sistema eólico empregando gerador de indução gaiola de esquilo. *Rev. Eletronica Potencia SOBRAEP* **23**, 330–338 (2018)
70. Yao, J.; Li, H.; Liao, Y.; Chen, Z.: An improved control strategy of limiting the DC-link voltage fluctuation for a doubly fed induction wind generator. *IEEE Trans. Power Electron.* **23**(3), 1205–1213 (2008)
71. Hopfensperger, B.; Atkinson, D.J.; Lakin, R.A.: Stator-flux-oriented control of a doubly-fed induction machine: with and without position encoder. *IEE Proceed.-Electr. Power Appl.* **147**(4), 241–250 (2000)
72. Tapia, G.; Tapia, A.; Ostolaza, J.X.: Proportional–integral regulator-based approach to wind farm reactive power management for secondary voltage control. *IEEE Trans. Energy Convers.* **22**(2), 488–498 (2007)
73. Rodriguez, J.; Kolar, J.; Espinoza, J.; Rivera, M.; Rojas, C.: Predictive torque and flux control of an induction machine fed by an indirect matrix converter with reactive power minimization. In: *IEEE International symposium on industrial electronics*, pp. 3177–3183 (2010).
74. Rivera, M.; Vargas, R.; Espinoza, J.; Rodríguez, J.; Wheeler, P.; Silva, C.: Current control in matrix converters connected to polluted AC voltage supplies. In: *IEEE power electronics specialists conference*. pp. 412–417 (2008).
75. Vargas, R.; Rodríguez, J.; Ammann, U.; Wheeler, P.W.: Predictive current control of an induction machine fed by a matrix converter with reactive power control. *IEEE Trans. Industr. Electron.* **55**(12), 4362–4371 (2008)
76. Ardjoun, S.A.E.M.; Denai, M.; Abid, M.: A robust power control strategy to enhance LVRT capability of grid-connected DFIG-based wind energy systems. *Wind Energy* **22**(6), 834–847 (2019)
77. Djeriri, Y.; Meroufel, A.; Massoum, A.; Boudjema, Z.: A comparative study between field oriented control strategy and direct power control strategy for DFIG. *J. Electr. Eng.* **14**(2), 9–9 (2014)
78. Hansen, A.D.; Michalke, G.: Fault ride-through capability of DFIG wind turbines. *Renew. Energy* **32**(9), 1594–1610 (2007)
79. Yang, X.; Liu, G.; Le, V.D.; Le, C.Q.: A novel model-predictive direct control for induction motor drives. *IEEE Trans. Electr. Electron. Eng.* **14**(11), 1691–1702 (2019)
80. Bouderbala, M.; Bossoufi, B.; Aroussi, H.A.; Taoussi, M.; Lagrioui, A.: Novel deadbeat predictive control strategy for DFIG's back to back power converter. *Int. J. Power Electron. Drive Syst.* **13**, 2731–2741 (2022)
81. Alami, H.E.; Bossoufi, B.; Mahfoud, M.E.; Bouderbala, M.; Majout, B.; Skruch, P.; Mobayen, S.: Robust Finite control-set model predictive control for power quality enhancement of a wind system based on the DFIG generator. *Energies* **16**(3), 1422 (2023)
82. Achar, A.; Djeriri, Y.; Benbouhenni, H.; Colak, I.; Oproescu, M.; Bizon, N.: Self-filtering based on the fault ride-through technique using a robust model predictive control for wind turbine rotor current. *Sci. Rep.* **14**(1), 1905 (2024). <https://doi.org/10.1038/s41598-023-51110-3>
83. Achar, A.; Djeriri, Y.; Benbouhenni, H.; Bentaallah, A.; Djehaf, M.A.; Hanafi, S.; Colak, I.: Robust Lyapunov-based power controllers with integral action for a wind farm. *Electr. Power Compon. Syst.* (2024). <https://doi.org/10.1080/1532500820242311880>

